Oligocene-Miocene back-thrusting in southern Mexico linked to the rapid subduction erosion of a large forearc block

D. Fraser Keppie,[1,2] A. J. Hynes,[2] J. K. W. Lee,[3] and M. Norman[4]

Received 28 June 2011; revised 5 January 2012; accepted 19 January 2012; published 21 March 2012.

[1] Both the timing and mechanism for the removal of a ~150–250 km wide forearc block from southern Mexico during the Cenozoic are controversial. Principal competing hypotheses are (1) removal due to sinistral strike-slip shear, in which slow, diachronous removal of the Chortis Block throughout the Cenozoic is inferred, and (2) removal due to subduction erosion, in which rapid removal of a large forearc block during the late Oligocene/early Miocene is inferred to be synchronous with the rapid landward migration of the southern Mexican arc. New data indicate northeast-directed back-thrusting in (1) the Chacalapa shear zone west of −96.5°E, with the timing of shear deformation bracketed by a 25.5 ± 0.5 Ma U/Pb zircon age and a 20.7 ± 0.6 Ma Ar/Ar biotite age, and (2) in an unnamed shear zone to the south, with the timing of deformation bracketed by a 27.5 ± 0.5 Ma U/Pb zircon age and a 25.1 ± 0.2 Ma Ar/Ar biotite age. Zircon and biotite ages date the emplacement and cooling of deformed plutons, respectively. The observed back-thrusting is consistent with a model of forearc removal due to subduction-erosion processes because it is evidence for subduction-orthogonal shortening occurring within the upper plate just before the landward migration of the southern Mexican arc. Rapid subduction of the southern Mexican forearc could have recycled continental lithosphere into the upper mantle at a rate up to half the global average rate of subduction erosion during the late Oligocene/early Miocene.

Citation: Keppie, D. F., A. J. Hynes, J. K. W. Lee, and M. Norman (2012), Oligocene-Miocene back-thrusting in southern Mexico linked to the rapid subduction erosion of a large forearc block, *Tectonics*, *31*, TC2008, doi:10.1029/2011TC002976.

1. Introduction

[2] Subduction zone processes represent a major part of the plate tectonic evolution of Earth. Subduction zones are respectively described as accretionary or erosive depending on whether continental material is added to or removed from the upper plate through time [*Scholl et al.*, 1980]. The importance of subduction erosion in shaping the tectonic evolution of active margins has become apparent in recent decades as studies now document the net removal of continental material in the majority of modern subduction zones [*Clift and Vannucchi*, 2004; *Clift et al.*, 2009; *Scholl and von Huene*, 2010]. Subduction erosion represents a major mechanism by which continental material may be recycled into the upper mantle [*Clift and Vannucchi*, 2004]. Where the Farallon and Nazca Plates have been subducting at the Pacific margin of South America, estimates for landward migration of the subduction interface due to subduction-erosion processes reach ~250 km for the lifetime of the convergent margin [*Kukowski and Oncken*, 2006; *Scholl and von Huene*, 2010,] (i.e., ~50–150 Ma). Most studies infer landward trench-migration rates due to subduction-erosion processes that are modest, typically ~2.5 km Ma^{-1}, and which are a small fraction of the associated rates of relative plate convergence [*Scholl and von Huene*, 2010]. The slow removal of forearc likely occurs due to the gradual weakening and detachment of material from the edge of the upper plate [*von Huene et al.*, 2004; *Kukowski and Oncken*, 2006], and has been dubbed edge-weakening subduction erosion [*D. F. Keppie et al.*, 2009] or ablative subduction erosion [*Tao and O'Connell*, 1992] in mechanical-modeling studies.

[3] In this context, forearc removal from southern Mexico would be notable because it could represent the most rapid subduction erosion of a forearc block yet documented in nature [*D. F. Keppie et al.*, 2009]. Removal of a ~150–250 km wide forearc block has been inferred from southern Mexico during the Cenozoic [*Karig et al.*, 1978; *Pindell et al.*, 1988; *Ross and Scotese*, 1988; *Morán-Zenteno et al.*, 1996; *J. D. Keppie et al.*, 2009]. The timing of forearc removal is likely constrained to be between ~27–25 Ma and 21–19 Ma by the paleo-position of the southern Mexican arc [*Morán-Zenteno et al.*, 1996; *J. D. Keppie et al.*, 2009]. Studies have variously favored three different removal mechanisms: (1) slow and diachronous removal of

[1]Department of Natural Resources, Halifax, Nova Scotia, Canada.
[2]Department of Earth and Planetary Sciences, McGill University, Montreal, Quebec, Canada.
[3]Department of Geological Sciences and Geological Engineering, Queen's University, Kingston, Ontario, Canada.
[4]Research School of Earth Sciences, Australian National University, Canberra, ACT, Australia.

0278-7407/12/2011TC002976

the missing forearc block, due to dextral strike-slip tectonics, predicting that Baja California is the missing forearc [*Karig et al.*, 1978]; (2) slow and diachronous removal of the missing forearc block, due to sinistral strike-slip tectonics, predicting that the Chortis Block is the missing forearc block [e.g., *Pindell et al.*, 1988; *Ross and Scotese*, 1988]; and (3) rapid subduction erosion of the missing forearc block, synchronous with the late Oligocene/early Miocene rapid landward migration of the southern Mexican arc [e.g., *Morán-Zenteno et al.*, 1996; *J. D. Keppie et al.*, 2009].

[4] These three models for forearc removal in southern Mexico have achieved different degrees of acceptance in the literature. In general, strike-slip removal has been favored [e.g., *Karig et al.*, 1978; *Pindell et al.*, 1988; *Morán-Zenteno et al.*, 2009]. Initially, the dextral model was preferred [*Karig et al.*, 1978], but this model has fallen out of favor since a late Cretaceous paleo-position for Baja California off western Mexico has been demonstrated [e.g., *Oskin et al.*, 2001; *Oskin and Stock*, 2003]. Subsequently, the sinistral model has been preferred [*Pindell et al.*, 1988; *Ross and Scotese*, 1988; *Rogers et al.*, 2007; *Silva-Romo*, 2008a; *Ratschbacher et al.*, 2009], which is consistent with a late Cretaceous Pacific origin for the Caribbean Plate relative to North and South America [*Pindell and Dewey*, 1982]. In this tectonic context, the Chortis Block might have been removed from southern Mexico as the Caribbean Plate migrated eastward relative to North and South America [*Pindell et al.*, 1988; *Ross and Scotese*, 1988; *Rogers et al.*, 2007; *Silva-Romo*, 2008a; *Ratschbacher et al.*, 2009]. However, rapid landward migration of the southern Mexican arc in the late Oligocene/early Miocene is inconsistent with a slow and diachronous model for forearc removal [*Morán-Zenteno et al.*, 2009; *D. F. Keppie et al.*, 2009; *J. D. Keppie et al.*, 2009]. Thus, a few studies have proposed that forearc removal in southern Mexico has been due to subduction-erosion processes [*Morán-Zenteno et al.*, 1996; *J. D. Keppie et al.*, 2009; *Morán-Zenteno et al.*, 2009].

[5] Previously, the ability to infer the rapid removal of a large forearc block due to subduction erosion processes has required the presence of a buoyant indentor on the lower plate arriving at the subduction zone to drive the rapid detachment and subduction of forearc material [*Chemenda et al.*, 1997a, 1997b; *Boutelier et al.*, 2003]. For southern Mexico, forearc removal due to subduction erosion has been considered unlikely because a buoyant indentor is not evident and the inferred total width of removed forearc ($\sim$250 km in 4–8 Ma [*Morán-Zenteno et al.*, 2009]), and the inferred rate of forearc removal ($\gg$20 km Ma^{-1} [*D. F. Keppie et al.*, 2009]) have been considered too large [e.g., *Silva-Romo*, 2008b]. Recent mechanical models indicate, however, that a fast mode of subduction erosion not requiring a buoyant indentor is also possible [*D. F. Keppie et al.*, 2009]. This fast mode occurs if the orogenic zone in the upper plate becomes weaker than the active subduction zone, so that subduction relocates into the weak orogenic zone [*D. F. Keppie et al.*, 2009]; this has been dubbed internal-weakening subduction erosion (IWSE) [*D. F. Keppie et al.*, 2009] or block subduction erosion (BSE) in mechanical modeling studies. For the IWSE/BSE mode, the intervening forearc is entrained and subducted with the lower plate at the rate of relative plate convergence [*D. F. Keppie et al.*, 2009]; as a result, IWSE/BSE could potentially subduct a >200 km wide forearc block in < 5 Ma, even assuming a relatively modest rate of relative plate convergence (>40 km Ma^{-1}), and thus might be the mode of forearc removal in the southern Mexican case [*D. F. Keppie et al.*, 2009].

[6] The purpose of this study is to test the different implications of the competing models of forearc removal in southern Mexico by documenting the timing and kinematics of shear deformation preserved in the present southern Mexican forearc. The essential hypothesis is that if plate-boundary deformation between the upper and lower plates across the Cenozoic southern Mexican subduction zone was not confined to a single shear zone, then synchronous dextral, sinistral, or orthogonal shear zones preserved in the remaining forearc would demonstrate the action of stresses consistent with the dextral, sinistral, or subduction-erosion models of forearc removal, respectively.

2. Geological Setting

[7] Forearc removal from southern Mexico is inferred for the ESE-trending margin extending from $\sim-105°$E to $\sim-95°$E (Figure 1) [e.g., *Karig et al.*, 1978; *Pindell et al.*, 1988; *Morán-Zenteno et al.*, 1996; *Silva-Romo*, 2008a]. The western part of this region comprises the southern portion of the Guerrero Terrane [*Campa and Coney*, 1983] and the eastern part comprises the Xolapa Complex along the coast and the Mixteca, Oaxaca, and Juarez Terranes to the north [*Campa and Coney*, 1983; *Keppie*, 2004].

[8] The Guerrero Terrane is composed of Mesozoic and Cenozoic volcanic and volcaniclastic rocks with both oceanic and continental affinities and a significant component of marine sedimentary rocks, possibly underlain by Precambrian basement [*Centeno-García et al.*, 1993, 2000]. The Xolapa Complex is a plutonic and metamorphic mid-crustal basement unit generally thought to represent a Jurassic through Cretaceous continental magmatic arc (JCMA) [*Herrmann et al.*, 1994]. Peak metamorphism in the Xolapa Complex produced extensive migmatitization at temperatures of $\sim$830–900°C and pressures of $\sim$630–950 MPa [*Corona-Chavez et al.*, 2006] between $\sim$160–90 Ma and 40–25 Ma [*Corona-Chavez et al.*, 2006; *Morán-Zenteno et al.*, 2007]. The Mixteca, Oaxaca, and Juarez Terranes consist broadly of Paleozoic, Proterozoic and Mesozoic rocks, respectively [*Campa and Coney*, 1983; *Keppie*, 2004], on which Jurassic red beds and Cretaceous limestones have been deposited [*Anderson and Schmidt*, 1983; *Freydier et al.*, 1997; *Filkorn*, 2003]. The boundaries between the Xolapa Complex and the northern terranes are generally defined by ductile shear zones or brittle faults, or are obscured by the intrusion of Cenozoic plutons [*Tolson et al.*, 1993; *Solari et al.*, 2007].

[9] Plutons intruding the basement terranes of southern Mexico range from $\sim$100 Ma in the Puerto Vallarta batholith to $\sim$25.5 Ma in the northern pluton on Rio San Francisco dated in this study [*Herrmann et al.*, 1994; *Ducea et al.*, 2004a; *Solari et al.*, 2007, this study]. A decrease in age of pluton emplacement from west to east from 100–40 Ma in the western part of the margin to 40–25.5 Ma in the eastern part of the margin has been suggested [*Schaaf et al.*, 1995; *Morán-Zenteno et al.*, 2007]. Pre-Cenozoic ages are found only west of $\sim-103°$E [*Morán-Zenteno et al.*, 2007]. East

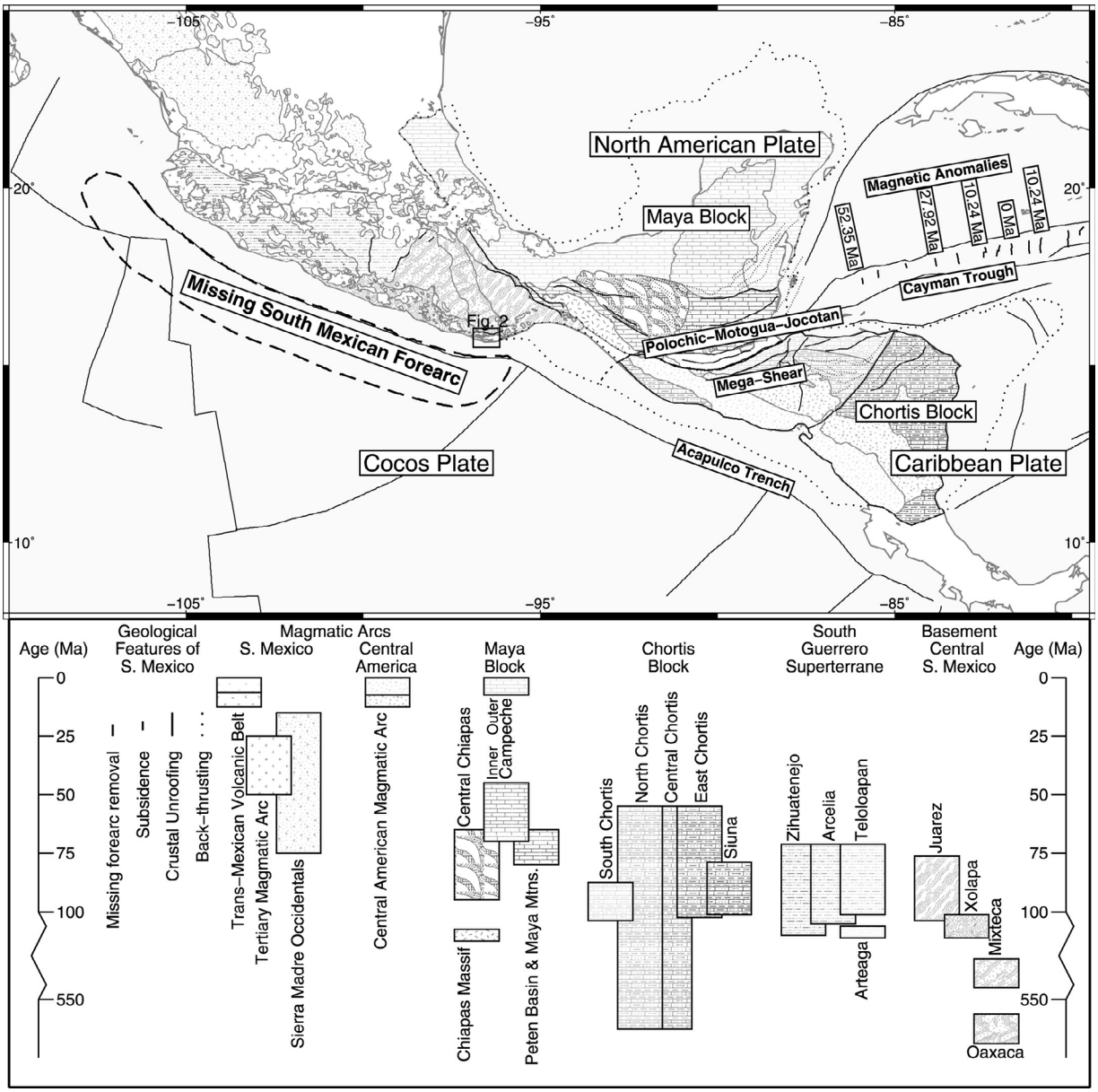

Figure 1. Geological and tectonic map of southern Mexico and the Chortis block. Structural lines and geological domains after *Becker et al.* [2009] (Regional), *Servicio Geológico Mexicano* [2007] and *Ferrari et al.* [1999a] (Mexico), *Purdy et al.* [2003] (Belize), *Weyl* [1980] (Guatemala), and *Rogers et al.* [2007] (Honduras). Terrane/fault block names for southern Mexico after *Keppie* [2004] and *Solari et al.* [2007] and in the Chortis block after *Rogers et al.* [2007].

of ∼−103°E, Cenozoic plutons comprise a Tertiary magmatic arc of Eocene to Miocene age along the modern coast of southern Mexico [*Morán-Zenteno et al.*, 1996]. Plutons in the Tertiary magmatic arc are generally undeformed granodiorites and tonalites, although granitic and dioritic compositions do occur [*Morán-Zenteno et al.*, 1996; *Ducea et al.*, 2004a; *Solari et al.*, 2007; *Morán-Zenteno et al.*, 2007]. Ductile shear zones have deformed the Tertiary magmatic arc in places [*Tolson*, 2005; *Solari et al.*, 2007].

[10] Plutons of the Tertiary magmatic arc and hosting country rocks may have been unroofed up to ∼10–20 km according to Al-in-amphibole geobarometry [*Morán-Zenteno et al.*, 1996]. Most of the unroofing likely occurred between the youngest ages of pluton emplacement in the Tertiary magmatic arc and mid-Miocene U/Th-He cooling ages recorded in zircons from these plutons [*Ducea et al.*, 2004b]. Magmatism ended in the Tertiary magmatic arc between ∼27 and 25 Ma [*Herrmann et al.*, 1994; *Ducea et al.*, 2004a; *Morán-Zenteno et al.*, 2007; this study]. Magmatism resumed in the Trans-Mexican Volcanic Belt (TMVB) in central Mexico as early as ∼21–19 Ma [*Ferrari et al.*, 1999a, 1999b; *Gómez-Tuena et al.*, 2008] and was widespread by ∼11–9 Ma [*Ferrari et al.*, 1999a]. Between 23.5 and 19 Ma, approximately 250 m of subsidence is documented from paleodepth estimates obtained from

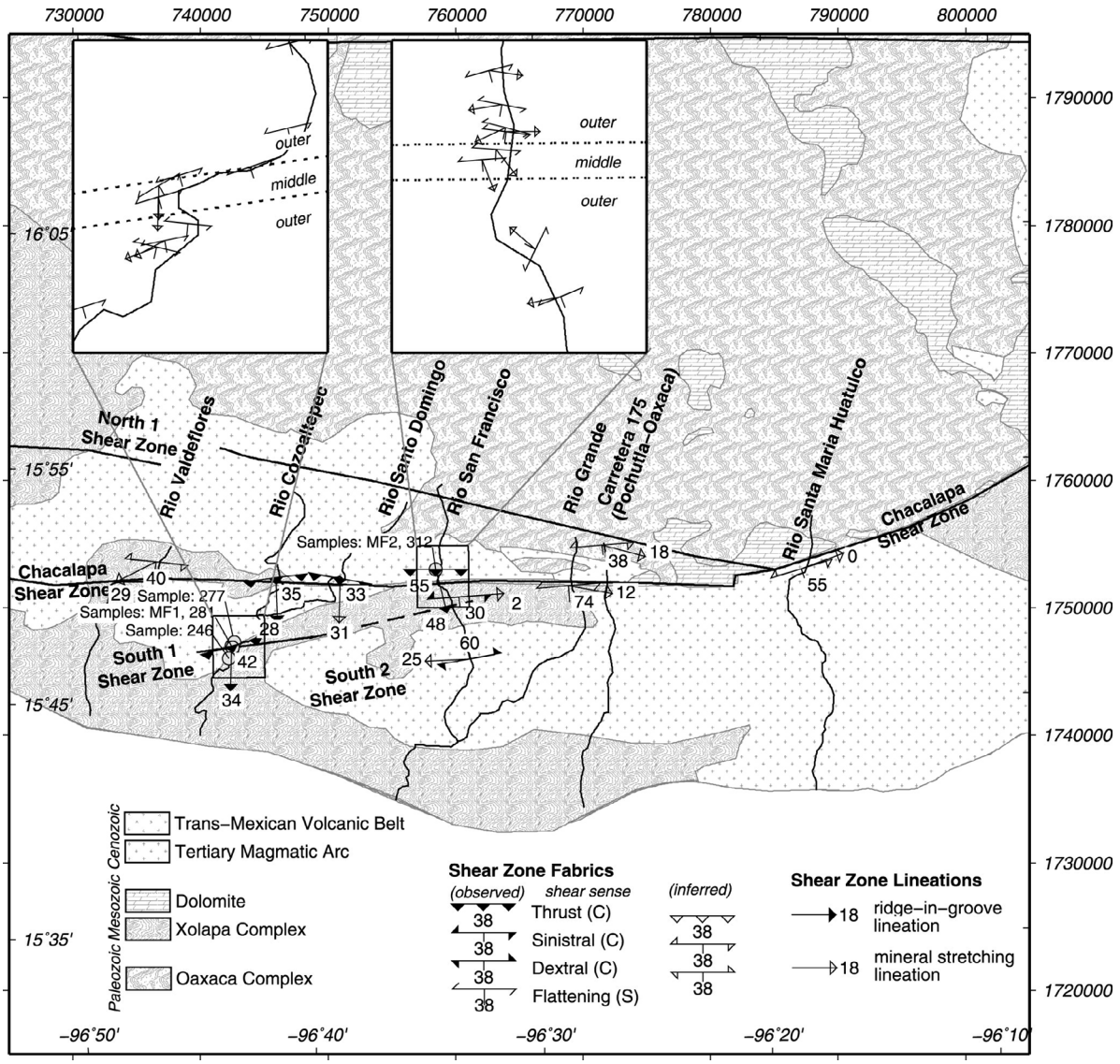

Figure 2. Geological location map for the study area showing representative structural data from observed shear zones. Main map shows shear (C) fabrics and shear directions. Insets show strikes of flattening (S) fabrics, trends of mineral stretching lineations, and definitions of middle and outer spatial domains related to the South 1 shear zone on Rio Cozoaltepec (left) and Chacalapa shear zone on Rio San Francisco (right).

submarine forearc sediments above the Acapulco Trench [*Clift and Vannucchi*, 2004].

3. Methods

3.1. Shear Zone Kinematic Analysis

[11] The full region to investigate, i.e., from ~−105°E to ~−95°E along the southern Mexican margin, is approximately 1000 km parallel and 100 km perpendicular to the Acapulco Trench, for a total area of 100, 000 km^2 (Figure 2). In this study, a small test area was chosen at the eastern end of this region (Figure 2). The chosen test area has two principal advantages compared with elsewhere: (1) it has extensive exposure of plutons of the Tertiary magmatic arc which could be expected to have been emplaced prior to, and deformed synchronous with, forearc removal, and (2) there are several evenly spaced S-trending rivers in the study area in which fresh outcrop surfaces are maintained despite the severe degradation resulting from tropical weathering evident elsewhere.

[12] All shear zones were analyzed to obtain as complete as possible a picture of strain partitioning within the study area [*Jiang et al.*, 2001]. Shear zones were assumed to be triclinic, in general, and middle and outer domains were defined and analyzed separately where possible [see *Jiang and Williams*, 1998]. Middle domains with a consistent shear fabric, shear direction and shear sense were assumed to reflect regions in which simple shear was dominant and vorticity number the highest [*Jiang and White*, 1995]. Deformation in outer domains was assumed to have been triclinic shear at smaller values of vorticity number, possibly dominated by the pure shear component; trends in the

variation of mineral stretching lineations passing from middle to outer domains were used to infer the character of the pure-shear component [see *Kuiper et al.*, 2007, 2011]. Within middle domains, shear directions were interpreted from ductile ridge-in-groove lineations where possible [see *Lin and Williams*, 1992; *Lin et al.*, 2007]. In their absence, the orthogonal projections of mineral-stretching lineations onto the shear fabric in high-strain zones were used when pseudo-monoclinic shearing could be assumed [see *Lin and Williams*, 1992; *Tikoff and Greene*, 1997]. Pseudo-monoclinic shearing was assumed when the lengths of long axes of stretched mineral grains were >40 times longer than the lengths of the short axes and the simple-shear component of strain likely dominated the pure-shear component of strain [*Lin et al.*, 2007]. Shear senses were interpreted from profiles of S-C fabrics, mica fish, rotated porphyroblasts with convincing tail geometries and Hansen fold-test criteria observed in the vorticity-normal surface [*Hansen*, 1971; *Passchier and Simpson*, 1986; *Jiang and White*, 1995; *Kuiper et al.*, 2007], where the vorticity-normal surface is the plane containing the shear direction and the pole to the shear (C) fabric [e.g., *Lin et al.*, 2007].

3.2. The $^{238}U/^{206}Pb$ Geochronology

[13] U/Pb zircon ages were obtained for selected samples (Figure 2). Samples 277 and 246 were collected from plutons deformed by the South 1 shear zone in Rio Cozoaltepec. Sample 313 was selected from an undeformed dyke cutting the South 1 shear zone in Rio Cozoaltepec. Sample 312 was collected from a pluton deformed by the Chacalapa shear zone in Rio San Francisco. Field samples were collected by sledgehammer and placed into clean 5 kg buckets. Individual pieces were washed and scrubbed with wire brush to remove any possible sediment contamination that might have been acquired during field handling. Zircon separates were obtained via stepwise crushing, heavy liquid separation, magnetic separation and hand-picking.

[14] Laser ablation inductively coupled plasma mass spectrometer (LA-ICPMS) analyses were conducted to obtain U/Pb systematics and trace element data for P, Ti, Y, Lu, Hf, Th, and U at the Australia National University [*Norman et al.*, 1996; *Cocherie and Robert*, 2008]. An EXCIMER UV laser system connected to an HP7500 Agilent mass spectrometer was used to analyze material from $\sim$50 μm pits. For each sample, a suite of single zircons was selected for analysis in order to obtain a representative profile of zircon age populations.

[15] The short half-life of ^{235}U ($\sim$704 Ma) means that several half-life cycles have been completed since the formation of Earth and isotopic abundances are generally insufficient to quantify ages from the $^{235}U/^{207}Pb$ system in geologically young mineral grains [*Jaffrey et al.*, 1971]. The half-life of ^{238}U is $\sim$4.47 Ga [*Jaffrey et al.*, 1971]. For the Mesozoic-Cenozoic plutons dated in this study, most of the age information is contained in the $^{238}U/^{206}Pb$ ratio [*Ludwig*, 2003]. We use the TuffZirc algorithm to extract reliable crystallization ages for populations of single-zircon $^{238}U/^{206}Pb$ ages [*Ludwig*, 2003].

[16] In the TuffZirc algorithm [*Ludwig*, 2003], analyses with anomalously high errors are removed from the age suite. The remaining analyses are then ranked according to $^{238}U/^{206}Pb$ age. The largest cluster of the ranked analyses that yields a probability-of-fit > 0.05 is then found. The true age is taken to be the median age of the largest cluster, without regard to analytical errors. The uncertainties are taken to be the (asymmetric) 95%-confidence errors of the median age. TuffZirc ages and their errors have been shown to be reliable using Monte Carlo testing, as long as > 40% of analyzed crystals are cogenetic with the main crystallization and free of Pb loss [*Ludwig*, 2003]. This is true even if the age suite contains xenocrysts only a few million years older than the main age of crystallization [*Ludwig*, 2003].

[17] Minimum estimates for the temperature of zircon crystallization may be calculated from the modified Ti-in-zircon geothermometer [*Ferry and Watson*, 2007]:

$$\log ppm_{Ti-in-zircon} = (5.711 \pm 0.0072) - (4800 \pm 86)/T(K) - \log a_{SiO_2} + \log a_{TiO_2} \quad (1)$$

In general, the Ti-in-zircon geothermometer has been shown to underestimate the crystallization temperature of zircon due to various effects [*Fu et al.*, 2008]. For example, an $a_{TiO_2} \approx 0.5$ can raise the calculated Ti-in-zircon temperature between 50 and 100°C [*Ferry and Watson*, 2007; *Fu et al.*, 2008]. When using the Ti-in-zircon geothermometer, the presence of rutile and titanite in the relevant sample is typically used to infer $a_{TiO_2} = 1.0$ and $a_{TiO_2} \approx 0.6 - 1.0$, respectively [*Ferry and Watson*, 2007; *Fu et al.*, 2008]. To a first approximation, however, a Ti-in-zircon temperature and a $^{238}U/^{206}Pb$ age provide a temperature-time point for the cooling and crystallization history of the associated pluton.

3.3. The $^{40}Ar/^{39}Ar$ Geochronology

[18] The $^{40}Ar/^{39}Ar$ amphibole and biotite ages were obtained for selected samples from sheared granitoid plutons (Figure 2). Samples MF1 and MF2 were selected from deformed plutons from the center of the South 1 and Chacalapa shear zones in Rio Cozoaltepec and Rio San Francisco, respectively. Hand samples were washed and scrubbed with a wire brush to remove any possible contamination that might have been acquired during field handling. Biotite and amphibole separates were obtained via crushing with a mortar-and-pestle, followed by ultrasonic cleaning and hand-picking under an optical microscope to obtain pure mineral separates. All analyses were carried out in the Queen's University ^{40}Ar-^{39}Ar geochronology laboratory. For each mineral separate, $\sim$5–10 mg of material were wrapped in Al foil and stacked vertically into Al canisters, which were then irradiated in the McMaster University Nuclear Reactor in Hamilton, Canada with the intralaboratory standard MAC-83 biotite at 24.36 Ma [*Sandeman et al.*, 1999] as referenced to TCR sanidine at 28.34 Ma and FCT sanidine at 28.201 Ma [*Kuiper et al.*, 2008]. Following irradiation, the samples and monitors were placed in small pits, $\sim$2 mm in diameter, drilled in a Cu sample holder. This was placed inside a small, bakeable, stainless steel chamber with a sapphire viewport connected to an ultra-high vacuum purification system. For each sample, step-heating experiments were conducted with an 8W Lexel 3500 continuous argon-ion laser with a defocused beam to degas Ar from 20–30 irradiated mineral grains of similar size in successive power steps for $\sim$3 min up to and including total melting. Monitors were fused in a single step. The evolved gases were purified using a SAES C50 getter

Table 1. Summary of Inferred Shear Zone Kinematics

River	Shear Zone	Representative Shear Fabric	Representative Shear Direction	Shear Sense Indicators C-S Fabrics	Mica Fish	(Sigma-type) Porphyroclasts
Valdeflores	Chacalapa	096/40	29@244			
Cozoaltepec	Chacalapa	083/35	28@178	thrust	thrust	80% thrust
Cozoaltepec	South 1	074/42	34@181	thrust	thrust	80% thrust
S. Domingo	Chacalapa	100/33	31@181	thrust		
S. Francisco	Chacalapa	090/55	48@165	thrust	thrust	75% thrust
S. Francisco	South 1	086/30	2@086			90% sinistral
S. Francisco	South 2	260/60	25@267			100% dextral
Grande	Chacalapa	085/74	12@100			
S.M. Huatulco	Chacalapa	073/55	0@070			

for ~5 min. Argon isotopes were measured using a MAP 216 mass spectrometer, with a Baur Signer source and an electron multiplier. All data were corrected for blanks, mass discrimination, atmospheric contamination, radioactive decay of ^{39}Ar, and neutron-induced interferences from K, Ca, and Cl [*Onstott and Peacock*, 1987; *Roddick*, 1983]. All ages are calculated using the decay constants recommended by *Steiger and Jager* [1977]. All quoted uncertainties are $\pm 2\sigma$, unless otherwise noted, and do not include errors in the decay constants.

[19] Closure temperatures [*Dodson*, 1973] were calculated for each sample using the Ar diffusion parameters of *Grove and Harrison* [1996] for biotite and *Harrison* [1981] for hornblende, the estimated grain size of the respective minerals in each rock as observed in thin section, and a rapid cooling rate of 40°C Ma^{-1} justified from iterative inspection of the geochronological data. Reported ^{40}Ar/^{39}Ar ages have been interpreted as cooling ages associated with the calculated closure temperatures [*Lee*, 1995].

4. Results

4.1. Shear Zone Kinematics

[20] Shear zone kinematics were obtained for nine outcrop sections (Table 1 and Figures 2 and 4). The inferred Chacalapa Shear Zone was identified and analyzed on six rivers, namely, from west to east, Rio Valdeflores, Rio Cozoaltepec, Rio Santo Domingo, Rio San Francisco, Rio Grande, and Rio Santa Maria Huatulco. The inferred South 1 Shear Zone was identified and analyzed on two rivers, namely, from west to east, Rio Cozoaltepec and Rio San Francisco. The inferred South 2 Shear Zone was identified and analyzed on Rio San Francisco. Within the study area, a further North 1 Shear Zone is reported in the latest regional geology map (Figure 2) [*Servicio Geológico Mexicano*, 2007], but was not independently visited or verified in this study.

[21] Lithologies in shear-zone sections were predominantly deformed granodioritic plutons with accessory biotite and amphibole, although slices of sedimentary host rocks are exposed in places within shear-zone sections. In the middle domains of the Chacalapa and South 1 Shear Zones, original igneous textures are mostly obscured due to mylonitization (Figure 3a). Recrystallized mineral assemblages are compatible with greenschist and lower amphibolite facies conditions: in detail, P-T conditions during shear are inferred from shear-related microstructures [*Tullis*, 2002]. Specifically, observations of boudinage in quartz layers between feldspar, and little phase mixing between adjacent quartz and mica, indicate minimum metamorphic conditions in the middle and upper-greenschist facies, and the complete recrystallization of quartz, the development of SC fabrics, and phase separation into banded mylonites indicate maximum metamorphic conditions in the upper-greenschist and lower-amphibolite facies [*Gapais*, 1989; *Tullis*, 2002]. Recrystallization and stretching lineations in quartz and feldspar crystals have long axes typically 40× longer (and often 70× longer) than shorter axes (Figure 3b). Alignment (and some stretching/growth) of amphibole crystals is also observed. Top-to-the-north, thrust sense of shear is indicated in most cases where S-C fabrics are developed (e.g., Figure 3c). Plagioclase porphyroclasts are typically ambiguous shear-sense indicators in these shear zones, but shear senses from the handful of porphyroclasts with well-developed σ-type tails [*Passchier and Simpson*, 1986] were identified and are compiled in Table 1. For the South 2 shear zone, shear fabrics and mineral lineations are much less well developed, with feldspar crystals showing only modest elongation (Table 1).

[22] For the Chacalapa Shear Zone west of −96.5°E, shear-zone kinematics are predominantly subduction-antithetic, dip-slip and thrust-sense (Figure 4). In contrast, for the Chacalapa Shear Zone east of −96.5°E, a sub-horizontal stretching lineation is predominant (Figure 4), and sinistral-sense, strike-slip kinematics have been inferred previously for this segment of the Chacalapa shear zone from microstructural analyses [*Tolson*, 2005]. On Rio Cozoaltepec, a relatively sharp strain gradient is observed at the northern margin of the Chacalapa shear zone, where granodiorite is transformed from an undeformed state to a pervasive mylonite over 1–10 m of continuous outcrop; a more gentle strain gradient is observed at the southern margin of the Chacalapa shear zone, where a similar change is observed over 200–300 m of regular, but discontinuous outcrop. In contrast, on Rio San Francisco, a relatively gentle strain gradient is observed at the northern margin of the Chacalapa shear zone with a transition from high to no deformation over ~1 km; passing from the middle domain to the outer domains, the predominant mineral stretching lineation switches progressively from margin-orthogonal, steeply plunging orientations to margin-parallel, shallowly plunging orientations over tens of meters, while flattening (S) fabrics retain a roughly constant orientation (Figure 2). The southern margin of the Chacalapa shear zone is not exposed on Rio San Francisco; the high-strain section extends for ~250 m normal to strike, where mylonitized granodiorite is then juxtaposed to a highly mylonitized and folded meta-

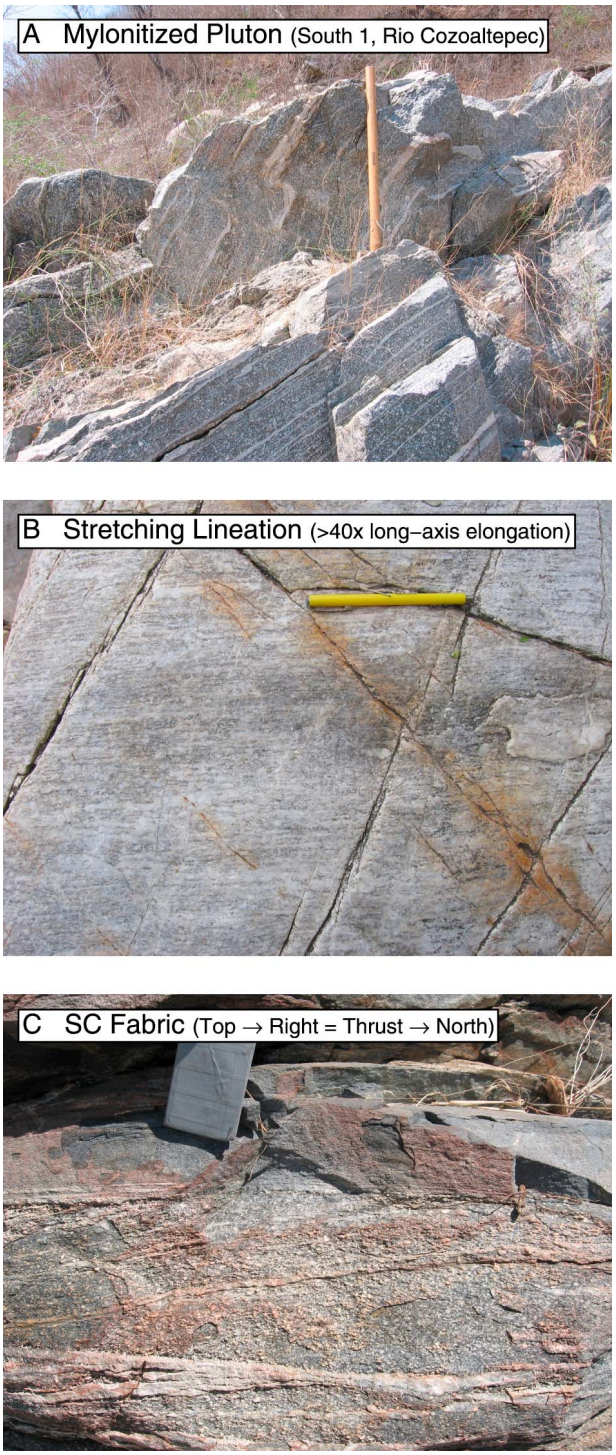

Figure 3. Field photos from the South 1 shear zone on Rio Cozoaltepec showing (a) mylonitization, (b) mineral stretching lineation, and (c) an SC-fabric kinematic indicator showing top to the right (i.e., thrusting to the north) sense of shear.

carbonate, followed by no outcrop. The middle domain of the Chacalapa Shear Zone appears to be <0.5 km wide normal to strike on all river traverses (Figure 2).

[23] The South 1 Shear Zone outcrops approximately 5 km and 1 km south of the Chacalapa Shear Zone on Rio Cozoaltepec and Rio San Francisco, respectively (Figure 2). Shear zone kinematics are predominantly subduction-antithetic, dip-slip and thrust-sense in the middle domain on the western Rio Cozoaltepec (Figure 3), but appear to be predominantly margin-parallel, strike-slip and sinistral-sense on the eastern Rio San Francisco (Figure 4). On Rio Cozoaltepec, the gradient from relatively undeformed to highly mylonitized at the northern margin of the South 1 Shear Zone is observed over ~300–500 m in regular, but discontinuous outcrop, and is accompanied by a steepening of mineral stretching lineations from margin-parallel, shallowly plunging orientations to margin-orthogonal, steeply plunging orientations sub-parallel to the inferred shear direction (Figure 2). On Rio San Francisco, the northern margin of the South 1 shear zone is truncated by a gabbroic pluton with cm- to dm-scale mineral grains at its base, grading rapidly through dioritic to granodioritic compositions with decreasing grain size going north. Extensive refolding of the mylonitic fabric is observed in the Rio San Francisco section of the South 1 Shear Zone. The strain gradient at the southern end of the South 1 shear zone is uncertain due in part to poor exposure. The South 1 Shear Zone appears to be ~0.5 km wide normal to strike on both river traverses.

[24] The South 2 Shear Zone outcrops approximately 5 km south of the South 1 Shear Zone on Rio San Francisco (Figure 2) and deforms a granite pluton with conspicuous 2–4 cm^3 sized plagioclase crystals. Mineral grains are aligned and the blocky plagioclase porphyroclasts (that were likely phenocrysts) show roughly 7:1 elongation ratios between long and short axes with parallelogram-like σ-type tails showing predominantly margin-parallel, strike-slip and dextral-sense deformation (Table 1). The South 2 shear zone outcrops sporadically over roughly 50 m normal to strike.

4.2. Shear Zone Geochronology

[25] Geochronological data reported here were collected from two of the shear zone sections described above, namely the South 1 Shear Zone on Rio Cozoaltepec and the Chacalapa Shear Zone on Rio San Francisco (Figure 2). These data are summarized in Tables 2 and 3 and Figures 5 and 6 for $^{238}U/^{206}Pb$ zircon and $^{40}Ar/^{39}Ar$ biotite and amphibole geochronology respectively. Presented ages and data reduction were derived using the Isoplot geochronology software [*Ludwig*, 2003]. Full isotopic and trace element laboratory analyses are included in Data Set S1 in the auxiliary material.[1]

[26] For the South 1 Shear Zone on Rio Cozoaltepec, zircons were dated from a finer-grained granodiorite in the high-strain zone (Sample 277), a lesser-deformed and coarser-grained granodiorite to the south of the high-strain zone (Sample 246), and an undeformed tonalitic dyke with large biotite crystals that cuts the high-strain zone (Sample 281). Also, amphibole and biotite were analyzed from highly mylonitized granodiorite in the center of the thrust-sense high-strain zone (sample MF1). Samples 277 and 246 yielded statistically significant TuffZirc $^{238}U/^{206}Pb$ zircon ages of 27.5 ± 0.5 Ma and 30.0 ± 0.3 Ma, respectively (Figures 5a and 5b). The zircon suites show clear young populations from which the crystallization ages are derived, and some inheritance of slightly older zircons.

[1] Auxiliary materials are available at ftp://ftp.agu.org/apend/tc/2011tc002976/.

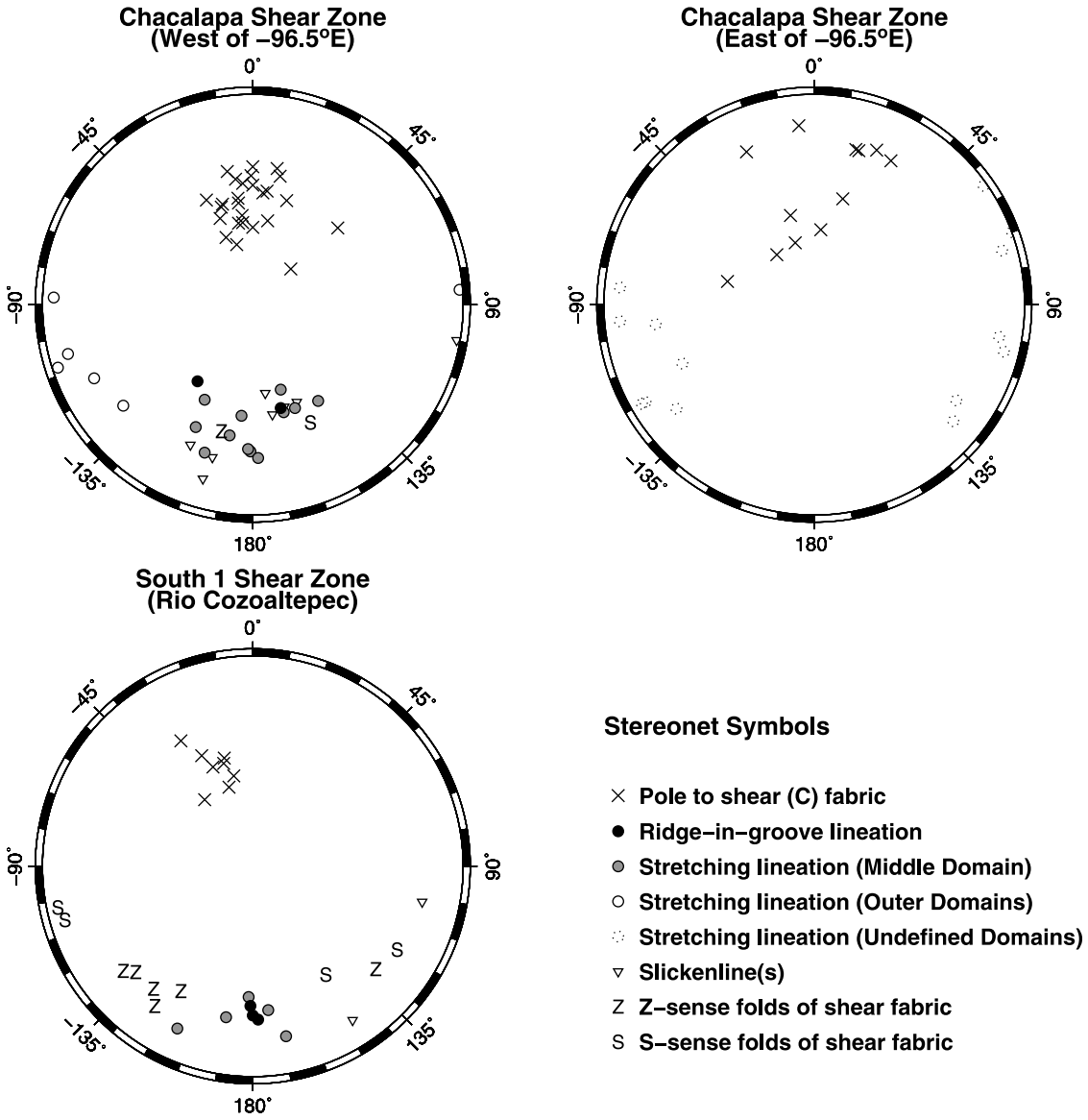

Figure 4. Summary of shear zone fabrics and lineations (Lambert Conformal Conic (Equal Area) projection).

Sample 246 yielded a TuffZirc $^{238}U/^{206}Pb$ zircon age of 29.5 ± 0.5 Ma (Figure 5c), although it is based on a coherence group of only 4 single-zircon ages (Table 2). The biotite $^{40}Ar/^{39}Ar$ age spectrum for Sample MF1 displays a very flat profile defining a plateau age of 25.14 ± 0.22 Ma over 98.6% of the ^{39}Ar released (MSWD = 0.46) (Figure 6a). The amphibole $^{40}Ar/^{39}Ar$ age spectrum for Sample MF1 displays a very flat profile defining a plateau age of 29.09 ± 0.47 Ma over 91.6% of the ^{39}Ar released (MSWD = 0.62) (Figure 6b).

[27] For the Chacalapa Shear Zone on Rio San Francisco, zircons (Sample 312), amphibole and biotite (Sample MF2) were dated for granodiorite from the same location in the center of the high-strain zone. Sample 312 yielded a statistically significant TuffZirc $^{238}U/^{206}Pb$ zircon age of 25.5 ± 0.5 Ma. The biotite $^{40}Ar/^{39}Ar$ age spectrum for Sample MF2 (Figure 6c) displays slightly younger apparent ages in the first 6.1% of ^{39}Ar released, suggestive of minor Ar loss as indicated by the corresponding Ca/K ratios (Data Set S1), but then reaches a plateau age of 20.70 ± 0.56 Ma over 93.9% of the ^{39}Ar released (MSWD = 0.39) (Figure 6c). The amphibole $^{40}Ar/^{39}Ar$ age spectrum for Sample MF2 (Figure 6d) displays anomalously old ages in the first two steps (≤2% of ^{39}Ar released), suggestive of Ar gain from other minor mineral phases as indicated by the corresponding Ca/K ratios (Data Set S1), but then falls to a well-defined plateau age of 27.93 ± 0.97 Ma over 98.1% of the ^{39}Ar released (MSWD = 0.31) (Figure 6d).

5. Discussion

5.1. Interpretation of Temperature-Time Data

[28] In Figure 7, we plot temperature-time data for each of the three minerals: zircon, amphibole, and biotite, determined for deformed plutons in the South 1 shear zone in Rio Cozoaltepec and the Chacalapa shear zone in Rio San

Table 2. Summary of LA-ICPMS U/Pb Zircon Geochronology

Sample	277	246	281	312
Traverse	Cozoaltepec	Cozoaltepec	Cozoaltepec	San Francisco
Shear Zone	South 1 (N-end)	South 1 (S-end)	South 1	Chacalapa
Shear Sense	thrust	thrust	thrust	thrust
Lithology	Granodiorite	Granodiorite	Tonalite	Granodiorite
Outcrop Type	Pluton	Pluton	Dyke	Pluton
Structure	Sheared	Sheared	Cross-cutting	Sheared
Longitude	W96d44m05.1s	W96d44m19.8s	W96d44m10.4s	W96d35m13.7s
Latitude	N15d47m32.8s	N15d46m52.7s	N15d47m19.8s	N15d50m33.5s
Easting	742670	742238	742499	758421
Northing	1747282	1746046	1746878	1753015
Analyses (tot)	19	24	12	24
Analyses (yng)	17	19	5	19
Age (Ma)	27.5	30	29.5	25.5
Sd*2	0.5	0.25	0.5	0.5
CI	94.30%	96.10%	87.80%	94.30%
Coherent group	14	12	4	14
Age (Ma)	27.8		29.0	26.2
Sd*2	0.42		1.70	1.00
MSWD	2.6		6.0	17.0
Average Ti (ppm)	4.3 ± 1.4	7 ± 2	10 ± 6	5.7 ± 1.3
Ti-in-zircon (°C)	669 ± 25	710 ± 26	729 ± 63	694 ± 18.8

Francisco. For zircon, we calculate a Ti-in-zircon temperature assuming $a_{SiO_2} = a_{TiO_2} = 1.0$ because quartz and titanite are present in the relevant samples and because this provides a minimum temperature estimate for the Ti-in-zircon geothermometer [*Fu et al.*, 2008]. In Figure 7, we correlate the U-Pb zircon ages with the Ti-in-zircon temperatures, but we acknowledge that this correlation may not be strictly justified due to differences in the U-Pb and Ti-in zircon systematics [*Fu et al.*, 2008]. Argon closure temperatures were calculated for each biotite and amphibole using an effective diffusion dimension equal to one-half of the actual grain size. For sample MF1, average biotite and amphibole grain sizes were 1.2 mm × 0.2 mm and 1.3 mm × 0.9 mm yielding closure temperatures of 373 ± 8°C and 598 ± 10°C, respectively. For sample MF2, average biotite and amphibole grain sizes were 0.4 mm × 0.1 mm and 1.5 mm × 1.1 mm yielding closure temperatures of 338 ± 8°C and 607 ± 9°C, respectively.

[29] For both shear zone sections, the simplest interpretation that is consistent with and supported by the temperature-time data in Figure 7 appears to be rapid cooling. Rapid cooling may have occurred in association with unroofing and exhumation of the plutons during shearing. In this interpretation, both the zircons and amphiboles likely formed during pluton crystallization, and the U-Pb age in the zircons and the Ar-closure age in the amphiboles provide estimates for the age of pluton emplacement. The slightly older ages for the amphiboles relative to the zircons is curious, but probably reflects the presence of excess radiogenic Ar that accumulated in the amphiboles from radiogenic Ar released from other minerals at depth. The Ar-closure ages in the biotites appear to provide estimates

Table 3. Summary of Step-Heating Ar/Ar Biotite and Amphibole Geochronology

Sample	MF1	MF1	MF2	MF2
Traverse	Cozoaltepec	Cozoaltepec	San Francisco	San Francisco
Shear Zone	South 1	South 1	Chacalapa	Chacalapa
Shear Sense	thrust	thrust	thrust	sinistral
Lithology	Granodiorite	Granodiorite	Granodiorite	Granodiorite
Mineral	Biotite	Amphibole	Biotite	Amphibole
Outcrop Type	Pluton	Pluton	Pluton	Pluton
Structure	Sheared	Sheared	Sheared	Sheared
Longitude	W96d44m16.1s	W96d44m16.1s	W96d35m13.7s	W96d35m13.7s
Latitude	N15d47m30.1s	N15d47m30.1s	N15d50m33.5s	N15d50m33.5s
Easting	742338	742338	758421	758421
Northing	1747194	1747194	1753015	1753015
Cooling Rate (°C Ma^{-1})	40	40	40	40
Average Grain Size (mm × mm)	1.2 × 0.2	1.3 × 0.9	0.4 × 0.1	1.5 × 1.1
Closure Temp (°C)	373 ± 8	598 ± 10	338 ± 8	607 ± 9
Plateau age (Ma)	25.14	29.09	20.70	27.93
Sd*2	0.22	0.47	0.56	0.97
J-error	0.003054	0.003050	0.003046	0.003043
MSWD	0.46	0.62	0.39	0.31
Confidence	0.95	0.60	0.95	0.91
%Ar39	98.6%	91.6%	93.9%	98.1%

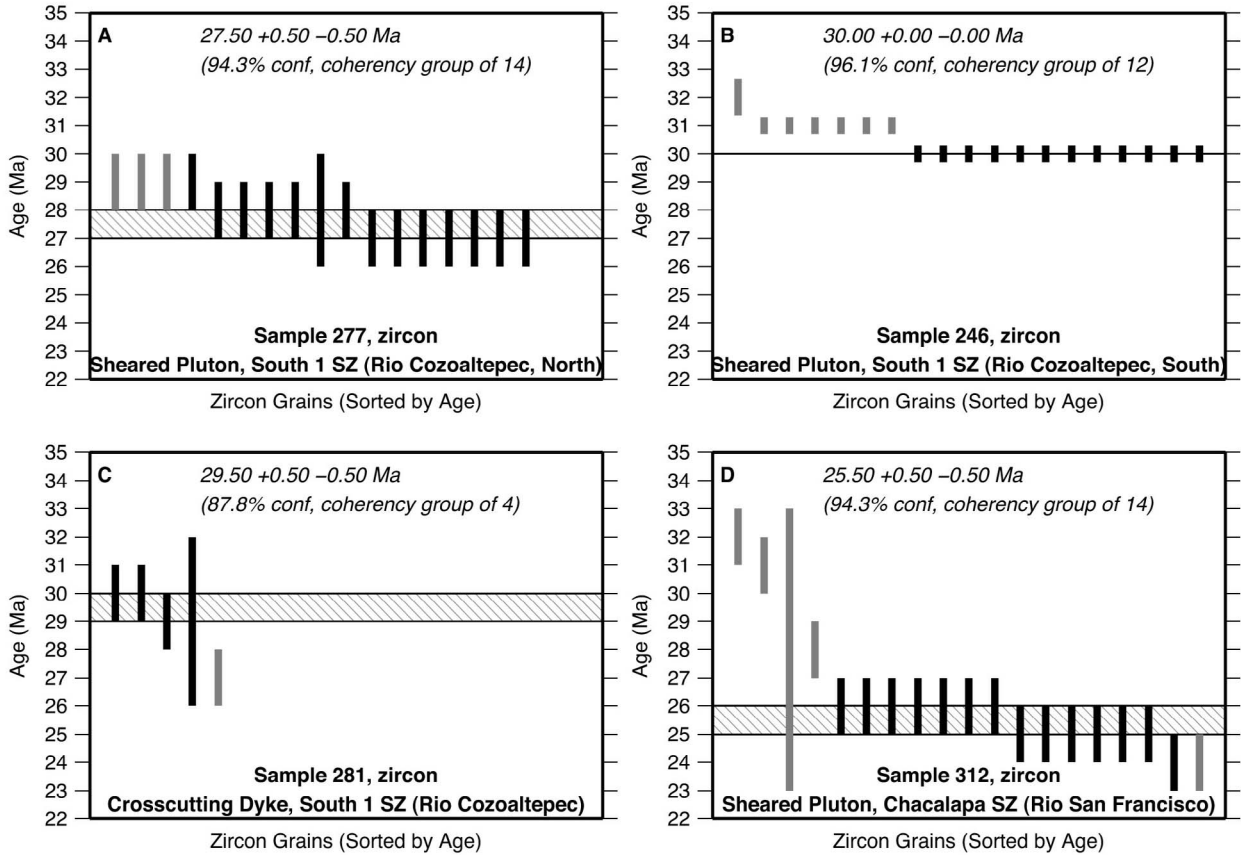

Figure 5. (a–d) TuffZirc $^{238}U/^{206}Pb$ cooling ages for single-zircon age populations. Vertical bars for samples included (black) or excluded (grey) from TuffZirc coherency group. Striped region shows age estimate. Error is 2σ.

for the minimum ages of shearing because shear zone textures indicate temperatures of shearing (i.e., ~400–600°C; Figure 7) that were above the Ar-closure temperatures for the biotites (i.e., 373 ± 8°C and 338 ± 8°C).

[30] Taken together, these data place very tight constraints on the timing and duration of shearing and suggest minimum average cooling rates of ~40°C Ma^{-1} for both shear zone sections (Table 3). Interpreted constraints on the temperature ranges of shearing are indicated with arrows to the right of the temperature time plot in Figure 7, and interpreted constraints on the age ranges of shearing are indicated with arrows above the temperature time plot in Figure 7. Constraints for the South 1 shear zone section on Rio Cozoaltepec are given with the black arrows and constraints on the Chacalapa shear zone section on Rio San Francisco are given with the grey arrows. Our interpretation is consistent with previous work, which brackets the age of the Chacalapa shear zone east of the present study area using a 29 ± 0.2 Ma U/Pb pluton emplacement age and a 23.7 ± 1.2 Ma K/Ar age for a cross-cutting dyke [*Tolson*, 2005]. U-Th/He data from zircons collected from Tertiary magmatic arc plutons near our study area also constrains unroofing of the coastal region to have been mostly complete by ~17.7–10.4 Ma [*Ducea et al.*, 2004a].

[31] The dyke cutting the fabric of deformed plutons in the South 1 shear zone on Rio Cozoaltepec yielded a 29.5 ± 0.5 Ma TuffZirc zircon age (Sample 281), which is older than the 27.5 ± 0.5 Ma zircon age obtained from one of the deformed plutons (Sample 277). To reconcile the structural and age data in this case, we infer that zircons in the dyke are xenocrysts inherited from slightly older nearby plutons, such as the pluton at the southern end of the shear zone dated to be ~30.0 Ma (Sample 246).

5.2. Interpretation of Kinematic Data

[32] We observe localized pseudo-monoclinic middle domains in the shear zones in the study area, with components of both subduction-antithetic dip-slip thrust-sense shearing and margin-parallel strike-slip sinistral shearing (Figures 2 and 4). Generally, this is consistent with strain-partitioning of the Cenozoic (Farallon) Cocos-North America relative convergence vector within the orogenic zone (Figure 8). Spatially, however, subduction-orthogonal shortening appears to predominate west of −96.5°E, whereas margin-parallel deformation appears to predominate east of −96.5°E. The transition in dominant shear sense appears to occur roughly where the margin boundary curves to the northeast just east of Punta Cometa (Figure 2), and thus could be a consequence of the change in margin azimuth.

[33] Within the study area, pseudo-monoclinic middle domains are best developed for the South 1 shear zone on Rio Cozoaltepec and the Chacalapa shear zone of Rio San

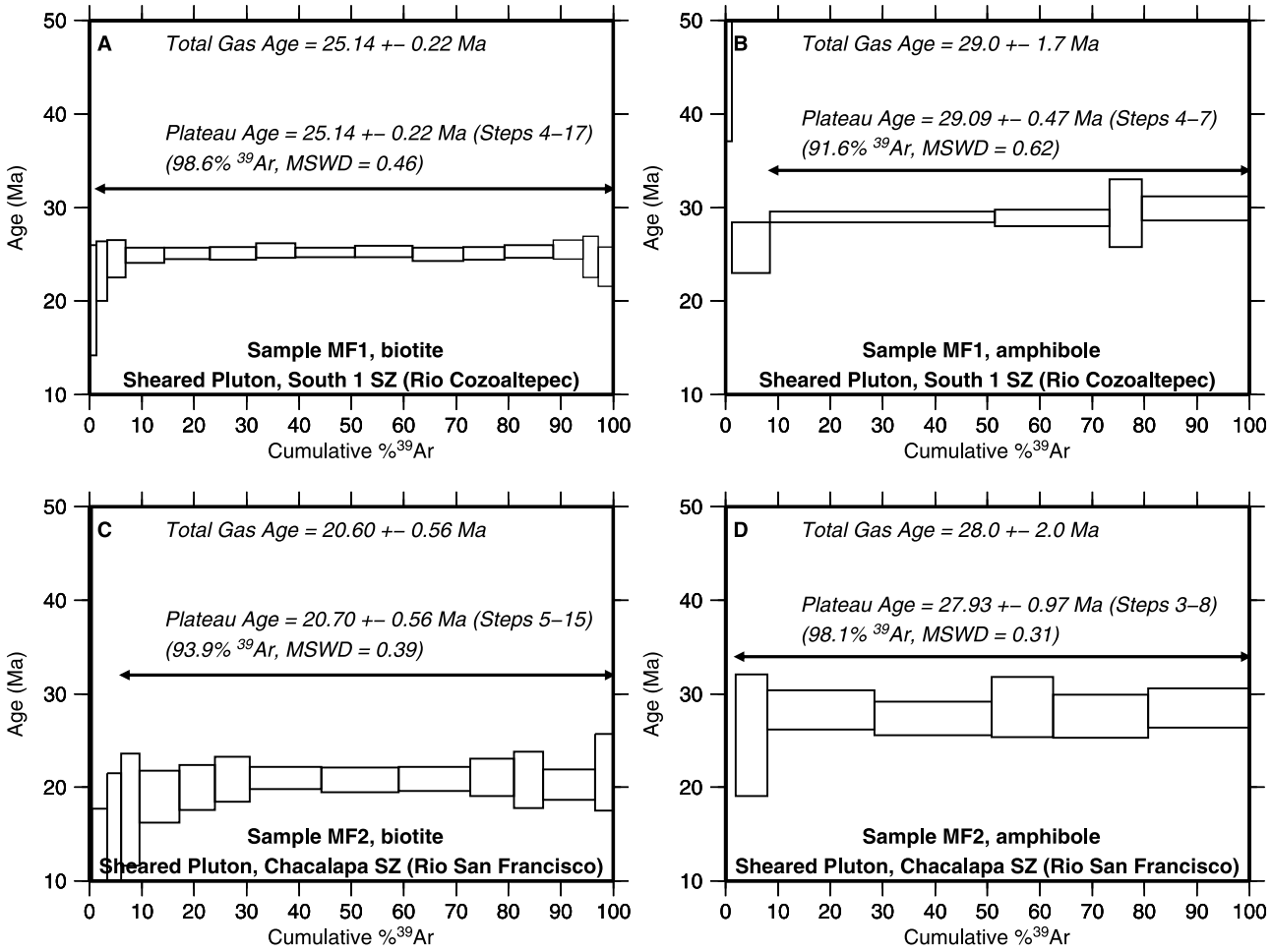

Figure 6. (a–d) The $^{40}Ar/^{39}Ar$ age spectra for biotites and amphiboles from samples MF1 and MF2. All uncertainties are $\pm 2\sigma$.

Francisco. In the middle domains, mineral stretching lineations are sub-parallel to the shear direction inferred from ridge-in-groove lineations, but become sub-horizontal as one passes from the middle domain to the outer domains. The simplest interpretation of these data is that both shear zones are triclinic, in general, but margin-perpendicular, thrust-sense, pseudo-monoclinic shearing was dominant in the middle domains, whereas orthorhombic, pure-shear components with margin-parallel extension were dominant in the outer domains [*Jiang*, 2007; *Kuiper et al.*, 2011]. In middle domains, finite strain was likely intermediate because mineral stretching lineations approximate the shear direction (Figure 4) [*Jiang*, 2007; *Kuiper et al.*, 2011].

[34] Shear zone traces inferred and plotted in Figure 2 correspond to shear zone traces reported on the latest regional geology map [*Servicio Geológico Mexicano*, 2007]. Note, however, that shear zone traces may differ from those plotted in Figure 2 because different shear zones intersect a given river traverse with a spacing of 1–10 km moving N-S, whereas the different river traverses cross the study area with a spacing of 2–20 km moving W-E. In an alternative scenario, a late Oligocene ENE-trending shear zone (South 1 + Chacalapa East) may have been cut by a slightly offset E-trending shear zone (Chacalapa West). The possibility also exists that the Chacalapa and South 1 shear zones on Rio San Francisco represent only a single > 2 km wide shear zone, if the undeformed diorite intruded between the two sections post-dates deformation. In contrast, the Chacalapa and South 1 shear zones on Rio Cozoaltepec likely represent two distinct thrust-sense zones because they are separated by a wide zone of almost continuous outcrop where deformation is less intense or absent. Since the South 1 thrusting event likely ended by $\sim$25.14 $\pm$ 0.22 Ma and Chacalapa thrusting likely ended by $\sim$20.70 $\pm$ 0.56 Ma, it is possible to speculate that subduction-orthogonal shortening propagated landward during the late Oligocene. Regardless of the nuances and possible ambiguities in their detailed interpretation, however, the geochronological and kinematic data reported here provide convincing evidence that subduction-orthogonal shortening modified the southern Mexican margin during a $\sim$5 Ma period spanning the late Oligocene and early Miocene.

[35] The South 2 shear zone had a notably different character to the Chacalapa and South 1 shear zones. Specifically, deformation in the South 2 shear zone appeared to be dextral and mineral stretching was limited to $\sim$10:1, which is substantially less than the > 40x mineral stretching observed in the Chacalapa and South 1 shear zones. Since relative plate motion between the Farallon-Cocos and North American Plates was mostly sinistral and convergent during the mid-

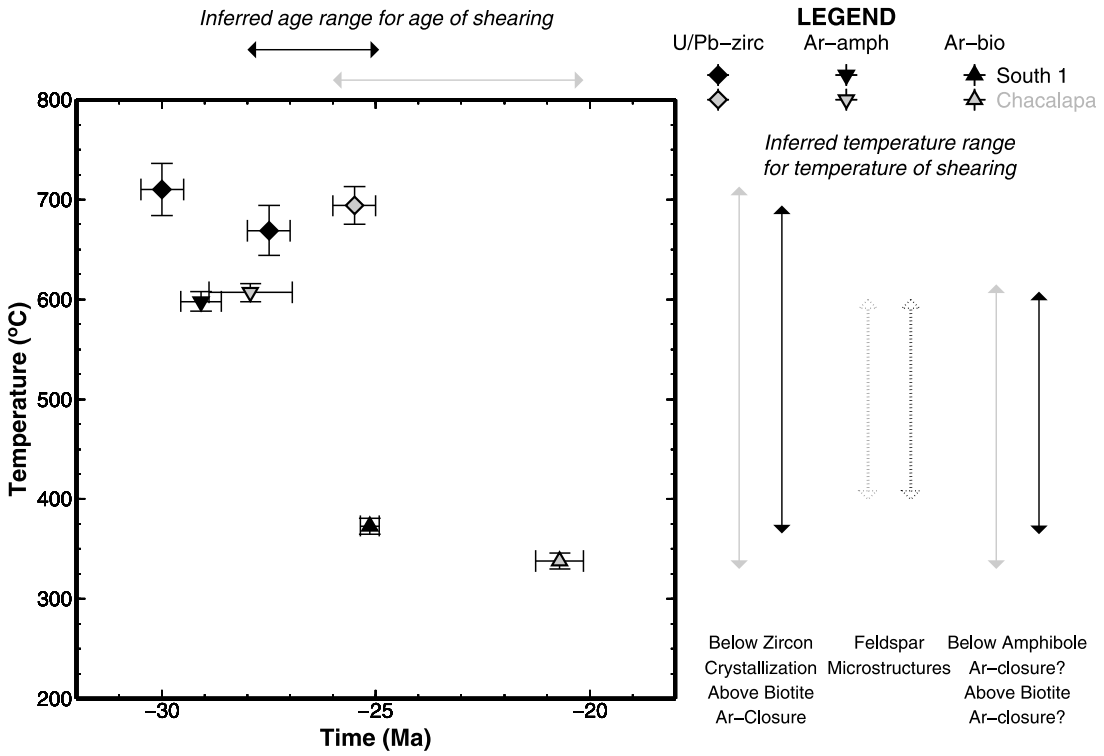

Figure 7. Temperature-time data for sheared plutons in southern Mexico. Zircon, amphibole, and biotite geochronology from Figures 5 and 6.

and late-Cenozoic (e.g., Figure 8), we infer that the South 2 shear zone was likely not involved in forearc removal processes acting during these times. Geochronological data partly testing this hypothesis will be published elsewhere.

5.3. Implications for the Mechanism of Forearc Removal

[36] As noted in the introduction, the purpose of this study was to test competing models of forearc removal from southern Mexico during the Cenozoic by identifying possibly correlative deformation in the present southern Mexican forearc. Our finding of thrust-sense, subduction-antithetic shearing on the Chacalapa and South 1 shear zones west of −96.5°E demonstrates the action of subduction-orthogonal shortening during the late Oligocene/early Miocene. Although this deformation might simply reflect general strain-partitioning within an orogenic zone, we suggest this deformation reflects the operation of internal-weakening or block subduction erosion (IWSE/BSE) along the southern Mexican margin at this time.

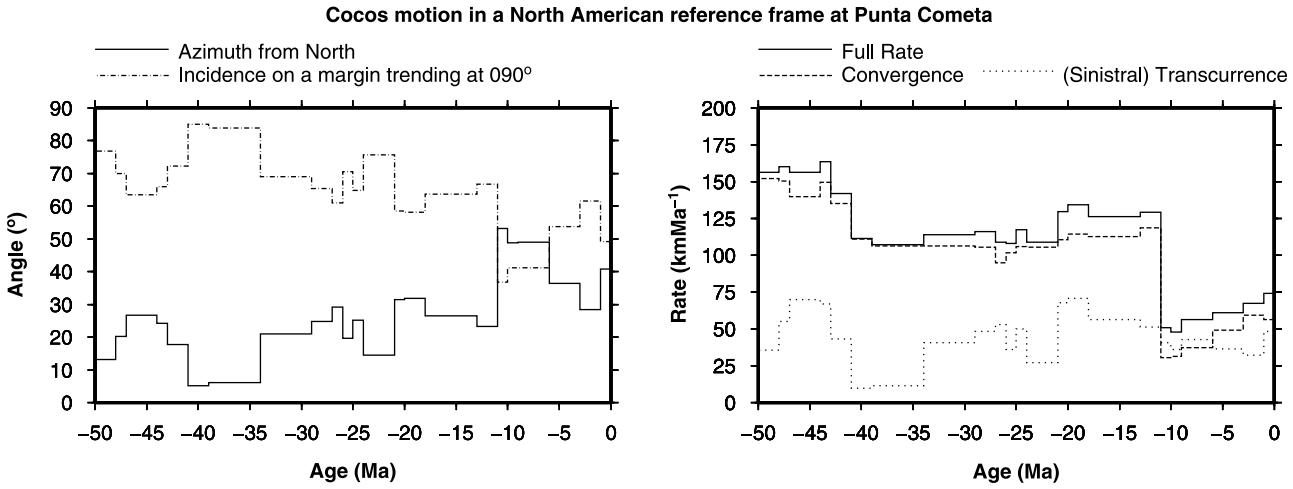

Figure 8. Relative convergence between (Farallon) Cocos and North America during the Cenozoic. In a North American reference frame: (left) azimuth from north and angle with respect to a 090°-trending margin, and (right) total, orthogonal and transcurrent relative motion rates.

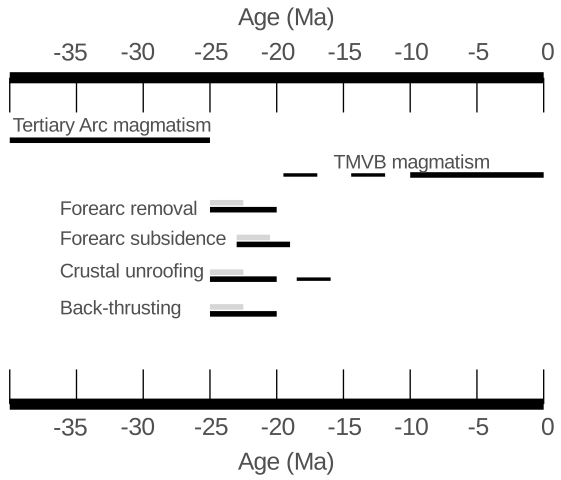

Figure 9. Age and lifespan constraints for geological features reported in southern Mexico (black) and those predicted by an internal-weakening subduction erosion mechanism of forearc removal (grey).

[37] The geology of southern Mexico records a remarkable set of broadly synchronous features (Figure 9): (1) a rapid, almost stepwise, shift in the locus of arc magmatism in southern Mexico from the Tertiary magmatic arc, ending at ~27–25 Ma, to the TMVB, starting at ~21–19 Ma [*Ferrari et al.*, 1999a, 1999b; *Gómez-Tuena et al.*, 2008]; (2) ~250 m of subsidence, between 23.5 and 20 Ma, immediately adjacent to the modern Acapulco Trench [*Clift and Vannucchi*, 2004]; (3) farther into the upper plate, a zone of 10–20 km of crustal unroofing of Tertiary magmatic arc plutons and surrounding country rocks prior to the middle Miocene [*Morán-Zenteno et al.*, 1996]; and (4) now, still farther inland, a zone of subduction-antithetic thrust-sense shear zones active at ~25–21 Ma synchronous with forearc removal (this study) and the subsidence in the trench.

[38] Collectively, these features may be explained by an IWSE/BSE event (Figure 10) [*D. F. Keppie et al.*, 2009]. Weakening in the orogenic zone leads to preferential partitioning of orthogonal stresses into the upper plate, represented initially by the formation of both subduction-synthetic and subduction-antithetic thrust zones. One of the subduction-synthetic thrust zones becomes the primary plate boundary, in which case the intervening forearc is entrained and subducted [*D. F. Keppie et al.*, 2009]. This may cause in turn (1) the rapid landward migration of the arc synchronous with the rapid landward migration of the trench [*D. F. Keppie et al.*, 2009], (2) a rapid period of continental shelf subsidence at the surface of Earth behind the departing forearc [*Clift and Vannucchi*, 2004], and (3) the unroofing and exhumation of the remaining forearc [*Morán-Zenteno et al.*, 1996] as the subducting forearc block acts like a buoyant indent or impinging on the upper plate across the new plate interface [*Warren et al.*, 2008a, 2008b]. Numerical models demonstrate the physical basis for the detachment and subduction of large forearc blocks from the margins of upper plates at the rates of relative plate convergence [*D. F. Keppie et al.*, 2009]. In southern Mexico, convergence rates of the Farallon-Cocos Plate relative to North America during the late Oligocene/early Miocene exceed ~100 km Ma^{-1} (Figure 8). Removal of the inferred 150–250 km wide forearc at rates above ~100 km Ma^{-1} indicates the proposed IWSE/BSE event could have taken place in ~1.5–2.5 Ma. This is in good agreement with the timing constraints obtained for the subduction-orthogonal shortening described in this study, as well as the other correlative geological phenomena noted above.

[39] In the absence of a IWSE/BSE event, it is not clear how any of these events is well-explained [*Morán-Zenteno et al.*, 2007; *J. D. Keppie et al.*, 2009]. Arc advance could accompany shallowing of the slab angle, but does not explain the wide arc widths of the Tertiary magmatic arc [*Morán-Zenteno et al.*, 2007]. Continental shelf subsidence could reflect edge-weakening or ablative subduction erosion (EWSE/ASE) [*Ducea et al.*, 2004b; *Clift and Vannucchi*, 2004], but then it is not clear why it is mostly confined to the early Miocene. Unroofing of the Xolapa complex and coastal Tertiary magmatic arc plutons would appear to need an as yet unidentified alternative mechanism [*J. D. Keppie et al.*, 2009].

5.4. Implications for Tectonic Models

[40] Our model that forearc removal from southern Mexico may have happened during the late Oligocene/early Miocene due to an IWSE/BSE event has implications for both regional and global tectonic models. Detailed discussion of these implications is beyond the scope of this study, but we briefly note the following.

[41] First, in most regional reconstructions, the late Oligocene paleo-position for the Chortis Block is south of the Isthmus of Tehuantepec [e.g., *Ross and Scotese*, 1988; *Rogers et al.*, 2007]. This position is immediately southeast of the region where we have inferred the existence of a large forearc block (subsequently subducted during an IWSE/BSE event). This could mean that the change in shear sense that we observe, from thrusting in the west to sinistral in the east, where shear zone traces bend to the northeast in our study area, corresponds to a change in the mechanism of forearc removal along the southern Mexican margin. On the other hand, transformation of plate-boundary deformation from shortening to shear is a necessary consequence of the observed change in plate boundary azimuth [*Wilson*, 1965]; thus independent data are needed to test whether these observations are related to a change in the mechanism of forearc removal.

[42] Second, in most regional reconstructions, the late Cretaceous paleo-position of the Chortis Block is in the Pacific Ocean south of the Acapulco Trench [e.g., *Ross and Scotese*, 1988; *Rogers et al.*, 2007]. If our model is correct, these reconstructions must be modified, as a minimum response, to accommodate the existence of a large forearc block off southern Mexico prior to the late Oligocene. If the large forearc block was in-place prior to the late Oligocene, the late Cretaceous position for the Chortis Block may have been along the southern margin of the forearc block rather than along the southern margin of modern Mexico. This possibility is interesting because it brings the two types of Pacific-origin model for the origin of the Caribbean Plate into closer agreement: Pacific-origin models based on a stable triple point at the northwest Caribbean Plate corner place the Chortis Block directly adjacent to the southern margin of the North American Plate [e.g., *Pindell and*

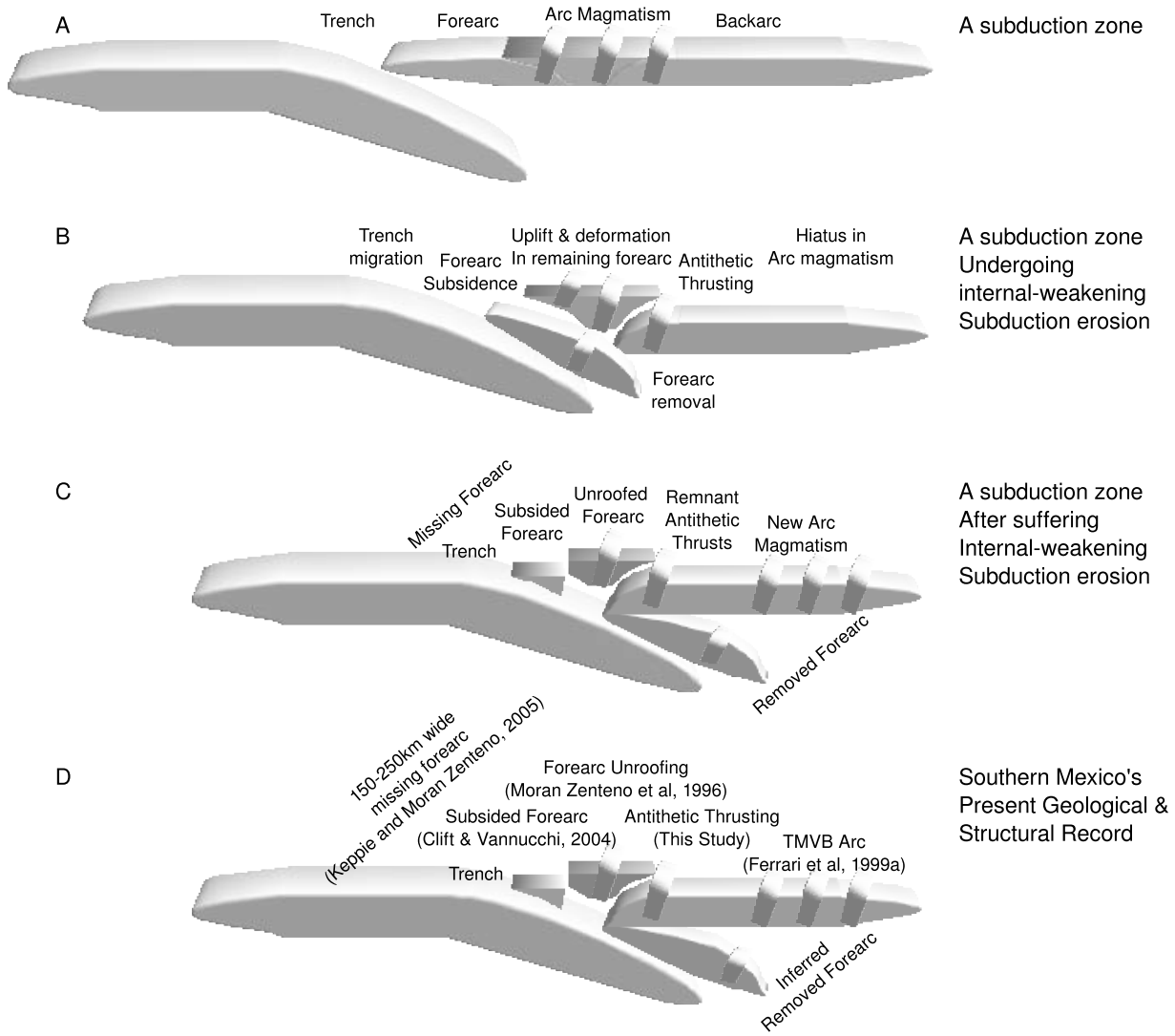

Figure 10. Schematic diagrams of (a) an initial subduction zone, (b) a subduction zone suffering internal-weakening subduction erosion, (c) a subduction zone after suffering internal-weakening subduction erosion, and (d) the geological record of southern Mexico.

Dewey, 1982; *Pindell and Kennan*, 2009], whereas Pacific-origin models based on a rigid Caribbean Plate place the Chortis Block some distance south of the modern margin of southern Mexico [e.g., *Wilson*, 1966; *Keppie and Morán-Zenteno*, 2005]. Alternatively, both the missing southern Mexico forearc and the Chortis Block could have been connected prior to the Oligocene and both moved southeastward together. An allochthonous model could be tested by evaluating whether the thrust deformation we describe here has overprinted earlier phases of sinistral shear. Overprinting is an alternative explanation for the margin-parallel, sub-horizontal mineral stretching lineations we observed in the outer domains of the Chacalapa and South 1 shear zones. For the Chortis Block, the main implication of this study is that forearc removal cannot be used to justify a paleoposition for the Chortis Block off southern Mexico during the late Cretaceous and early Cenozoic because the Chortis Block may not be the removed forearc [*Keppie and Morán-Zenteno*, 2005].

[43] Third, the emergence of the Trans-Mexican Volcanic Belt across Central Mexico may be causally related to the IWSE/BSE event inferred here. In this scenario, the arc may have resumed in a relatively landward position following the landward migration of the trench due to subduction erosion [*D. F. Keppie et al.*, 2009]. This possibility must be considered when discussing the possible mechanisms of arc initiation for the Trans-Mexican Volcanic Belt, which include tearing of the Cocos slab [*Ferrari*, 2004] and/or viscosity changes in the mantle wedge immediately above the Cocos slab [*Manea and Gurnis*, 2007]. Studies evaluating how much subducted crust may have existed in the source regions for the oldest volcanics in the Trans-Mexican Volcanic Belt [e.g., *Petrone and Ferrari*, 2008] may help to identify the role played by an IWSE/BSE event, if any.

[44] Finally, the present estimate for the average global Cenozoic rate of continental lithosphere recycling due to subduction erosion processes is $\sim$1.3 km^3 Ma^{-1} [*Clift et al.*, 2009]). The IWSE/BSE event inferred here could have involved the subduction of a forearc block with approximate

average dimensions of ~10 × 1000 × 150–250 km^3 (depth × length × width) in <5 Ma. If so, this event may represent an additional contribution of ~20% to 50% of the average global rate during the late Oligocene/early Miocene. Internal-weakening or block subduction erosion events may represent important contributions for global models of continental lithosphere recycling.

6. Conclusions

[45] Partitioning of the Cocos-North America oblique convergence vector occurred on localized high strain thrust-sense and sinistral-sense shear zones in southern Mexico during the late Oligocene and early Miocene. In the study area, the southern South 1 subduction-antithetic thrust-sense shear zone was active until ~25.14 ± 0.22 Ma and the northern Chacalapa subduction-antithetic thrust-sense shear zone was active until ~20.60 ± 0.56 Ma. Subduction-antithetic thrust-sense shearing was synchronous with the timing of removal of a 150–250 km wide forearc block from southern Mexico. These features may be related and explained if forearc removal from southern Mexico occurred due to internal-weakening or block subduction erosion resulting in the recycling of a significant volume of continental lithosphere during the Cenozoic.

[46] **Acknowledgments.** D.F.K. acknowledges (1) The National Autonomous University of Mexico (UNAM) for providing logistical field support including the use of a truck; (2) Kerry Klein, Hector Hinojosa, and Carl Nagy for their field assistance in Mexico; (3) students at UNAM, Australia National University (ANU) and Queens University for helping during various stages of processing geochronological samples; (4) Herbert Fournier and Douglas Archibald for their teaching, supervision, and help processing Ar geochronology samples at Queen's University; and (5) financial support from NSERC Canada and a Tomlinson Fellowship at McGill. J.K.W.L. acknowledges support from both Natural Sciences and Engineering Research Council of Canada (NSERC) Discovery and Major Research Support grants.

References

Anderson, T. H., and V. A. Schmidt (1983), The evolution of Middle America and the Gulf of Mexico-Caribbean Sea region during Mesozoic time, *Geol. Soc. Am. Bull.*, *94*, 941–966.

Becker, J. J., et al. (2009), Global bathymetry and elevation data at 30 arc seconds resolution: SRTM30_PLUS, *Mar. Geod.*, *32*, 355–371.

Boutelier, D., A. Chemenda, and J.-P. Burg (2003), Subduction versus accretion of intra-oceanic volcanic arcs: insight from thermo-mechanical analogue experiments, *Earth Planet. Sci. Lett.*, *212*, 31–45.

Campa, M., and P. Coney (1983), Tectono-stratigraphic terranes and mineral resource distributions in Mexico, *Can. J. Earth Sci.*, *20*, 1040–1051.

Centeno-García, E., J. Ruiz, P. J. Coney, P. J. Patchett, and F. Ortega-Gutierrez (1993), Guerrero terrane of Mexico: Its role in the southern Cordillera from new geochemical data, *Geology*, *21*(5), 419–422.

Centeno-García, E., M. Guerrero-Suastegui, and O. Talavera-Mendoze (2000), The Guerrero composite terrane of western Mexico: Collision and subsequent rifting in a supra-subduction zone, in *Formation and Applications of the Sedimentary Record in Arc Collision Zones*, edited by A. E. Draut, P. D. Clift, and D. W. Scholl, *Spec. Pap. Geol. Soc. Am.*, *436*, 279–308.

Chemenda, A., P. Matte, and V. Sokolov (1997a), A model of Palaeozoic obduction and exhumation of high-pressure/low-temperature rocks in the southern Urals, *Tectonophysics*, *276*, 217–227.

Chemenda, A., R. Yang, C.-H. Hsieh, and A. Groholsky (1997b), Evolutionary model for the Taiwan collision based on physical modelling, *Tectonophysics*, *274*, 253–274.

Clift, P., and P. Vannucchi (2004), Controls on tectonic accretion versus erosion in subduction zones: Implications for the origin and recycling of the continental crust, *Rev. Geophys.*, *42*, RG2001, doi:10.1029/2003RG000127.

Clift, P. D., P. Vannucchi, and J. P. Morgan (2009), Crustal redistribution, crust-mantle recycling and phanerozoic evolution of the continental crust, *Earth Sci. Rev.*, *97*, 80–104, doi:10.1016/j.earscirev.2009.10.003.

Cocherie, A., and M. Robert (2008), Laser ablation coupled with ICP-MS applied to U-Pb zircon geochronology: A review of recent advances, *Gondwana Res.*, *14*, 597–608.

Corona-Chavez, P., S. Poli, and B. Bigioggero (2006), Syn-deformational migmatities and magmatic-arc metamorphism in the Xolapa Complex, southern Mexico, *J. Metamorph. Geol.*, *24*, 169–191, doi:10.1111/j.1525-1314.2006.00632.x.

Dodson, M. H. (1973), Closure temperature in cooling geochronological and petrological systems, *Contrib. Mineral. Petrol.*, *40*(3), 259–274, doi:10.1007/BF00373790.

Ducea, M. N., G. E. Gehrels, S. Shoemaker, J. Ruiz, and V. A. Valencia (2004a), Geologic evolution of the Xolapa complex, southern Mexico: Evidence from U-Pb zircon geochronology, *Geol. Soc. Am. Bull.*, *116*, 1016–1025, doi:10.1130/B25467.1.

Ducea, M. N., V. A. Valencia, S. Shoemaker, P. W. Reiners, P. G. DeCelles, M. F. Campa, D. Moran-Zenteno, and J. Ruiz (2004b), Rates of sediment recycling beneath the Acapulco trench: Constraints from (U-Th)/He thermochronology, *J. Geophys. Res.*, *109*, B09404, doi:10.1029/2004JB003112.

Ferrari, L. (2004), Slab detachment control on mafic volcanic pulse and mantle heterogeneity in central Mexico, *Geology*, *32*(1), 77–80, doi:10.1130/G19887.1.

Ferrari, L., M. López-Martínez, G. Aguirre-Díaz, and G. Carrasco-Núñez (1999a), Space-time patterns of Cenozoic arc volcanism in central Mexico: From the Sierra Madre Occidental to the Mexican volcanic belt, *Geology*, *27*, 303–306.

Ferrari, L., G. Pasquaré, S. Venegas-Salgado, and F. Romero-Rios (1999b), Geology of the western Mexican volcanic belt and adjacent Sierra Madre Occidental and Jalisco block, in *Cenozoic Tectonics and Volcanism of Mexico*, edited by H. Delgado-Granados, G. J. Aguirre-Díaz, and J. M. Stock, *Spec. Pap. Geol. Soc. Am.*, *334*, 65–83.

Ferry, J. M., and E. B. Watson (2007), New thermodynamic models and revised calibrations for the Ti-in-zircon and Zr-in-rutile thermometers, *Contrib. Mineral. Petrol.*, *154*, 429–437, doi:10.1007/s00410-007-0201-0.

Filkorn, H. F. (2003), The Cretaceous corals of Mexico: Occurrences and history of research, *Rev. Mex. Cienc. Geol.*, *20*(1), 52–78.

Freydier, C., H. Lapierre, L. Briqueu, M. Tardy, C. Coulon, and J. Martinez-Reyes (1997), Volcaniclastic sequences with continental affinities within the late Jurassic-early Cretaceous Guerrero intra-oceanic arc terrane (Western Mexico), *J. Geol.*, *105*, 483–502.

Fu, B., F. Z. Page, A. J. Cavosie, J. Fournelle, N. T. Kita, J. S. Lackey, S. A. Wilde, and J. W. Valley (2008), Ti-in-zircon thermometry: Applications and limitations, *Contrib. Mineral. Petrol.*, *156*, 197–215, doi:10.1007/s00410-008-0281-5.

Gapais, D. (1989), Shear structures within deformed granites: Mechanical and thermal indicators, *Geology*, *17*, 1144–1147, doi:10.1130/0091-7613(1989)017<1144:SSWDGM>2.3.CO;2.

Gómez-Tuena, A., L. Mori, N. E. Rincón-Herrera, F. Ortega-Gutiérrez, J. Solé, and A. Iriondo (2008), The origin of a primitive trondhjemite from the Trans-Mexican volcanic belt and its implications for the construction of a modern continental arc, *Geology*, *36*, 471–474, doi:10.1130/G24687A.1.

Grove, M., and T. Harrison (1996), ^{40}Ar diffusion in Fe-rich biotite, *Am. Mineral.*, *81*, 940–951.

Hansen, E. (1971), *Strain Facies*, Springer, Berlin.

Harrison, T. (1981), Diffusion of ^{40}Ar in hornblende, *Contrib. Mineral. Petrol.*, *78*, 324–331.

Herrmann, U. R., B. K. Nelson, and L. Ratschbacher (1994), The origin of a terrane: U/Pb zircon geochronology and tectonic evolution of the Xolapa complex (southern Mexico), *Tectonics*, *13*, 455–474, doi:10.1029/93TC02465.

Jaffrey, A., K. Flynn, L. Glendenin, W. Bentley, and A. Essling (1971), Precision measurement of half-lives and specific activities of ^{235}U and ^{238}U, *Phys. Rev. C*, *4*(5), 1889–1906, doi:10.1103/PhysRevC.4.1889.

Jiang, D. (2007), Sustainable transpression: An examination of strain and kinematics in deforming zones with migrating boundaries, *J. Struct. Geol.*, *29*, 1984–2005, doi:10.1016/j.jsg.2007.09.007.

Jiang, D., and J. C. White (1995), Kinematics of rock flow and the interpretation of geological structures, with particular reference to shear zones, *J. Struct. Geol.*, *17*, 1249–1265.

Jiang, D., and P. F. Williams (1998), High-strain zones: A unified model, *J. Struct. Geol.*, *20*, 1105–1120, doi:10.1016/S0191-8141(98)00025-X.

Jiang, D., S. Lin, and P. Williams (2001), Deformation path in high-strain zones, with reference to slip partitioning in transpressional plate-boundary zones, *J. Struct. Geol.*, *23*, 991–1005.

Karig, D. E., R. Cardwell, G. Moore, and D. Moore (1978), Late Cenozoic subduction and continental margin truncation along the northern Middle America trench, *Geol. Soc. Am. Bull.*, *89*, 265–276.

Keppie, D. F., C. A. Currie, and C. Warren (2009), Subduction erosion modes: comparing finite element numerical models with the geological record, *Earth Planet. Sci. Lett.*, *287*, 241–254.

Keppie, J. D. (2004), Terranes of Mexico revisited: A 1.3 billion year odyssey, *Int. Geol. Rev.*, *46*, 765–794.

Keppie, J. D., and D. J. Morán-Zenteno (2005), Tectonic implications of alternative Cenozoic reconstructions for southern Mexico and the Chortis block, *Int. Geol. Rev.*, *47*, 473–491.

Keppie, J. D., D. J. Moran-Zenteno, B. Martiny, and E. Gonzalez-Torres (2009b), Synchronous 29–19 Ma arc hiatus, exhumation and subduction of forearc in southwestern Mexico, in *The Origin and Evolution of the Caribbean Plate*, edited by K. H. James, M. A. Lorente, and J. L. Pindell, *Geol. Soc. Spec. Publ.*, 328, 169–179, doi:10.1144/SP328.7.

Kuiper, K., A. Deino, F. Hilgen, W. Krijgsman, P. Renne, and J. Wijbrans (2008), Synchronizing rock clocks of earth history, *Science*, *320*, 500–504.

Kuiper, Y. D., D. Jiang, and S. Lin (2007), Relationship between non-cylindrical fold geometry and the shear direction in monoclinic and triclinic shear zones, *J. Struct. Geol.*, *29*, 1022–1033.

Kuiper, Y. D., S. Lin, and D. Jiang (2011), Deformation partitioning in transpressional shear zones with an along-strike stretch component: An example from the superior boundary zone, Manitoba, Canada, *J. Struct. Geol.*, *33*, 192–202, doi:10.1016/j.jsg.2010.07.003.

Kukowski, N., and O. Oncken (2006), Subduction erosion—The "normal" mode of fore-arc material transfer along the Chilean margin?, in *The Andes: Active Subduction Orogeny*, *Front. Earth Sci. Ser.*, vol. 1, edited by O. Oncken et al., pp. 217–236, Springer, Berlin.

Lee, J. K. (1995), Multipath diffusion in geochronology, *Contrib. Mineral. Petrol.*, *120*, 60–82.

Lin, S., and P. F. Williams (1992), The geometrical relationship between the stretching lineation and the movement direction of shear zones, *J. Struct. Geol.*, *14*, 491–497.

Lin, S., D. Jiang, and P. F. Williams (2007), Importance of differentiating ductile slickenside striations from stretching lineations and variation of shear direction across a high-strain zone, *J. Struct. Geol.*, *29*, 850–862.

Ludwig, K. R. (2003), User's manual for Isoplot/Ex, version 3.0: A geochronological toolkit for Microsoft Excel, *Spec. Publ. 4*, 71 pp., Berkeley Geochron. Cent., Berkeley, Calif.

Manea, V., and M. Gurnis (2007), Subduction zone evolution and low viscosity wedges and channels, *Earth Planet. Sci. Lett.*, *264*, 22–45, doi:10.1016/j.epsl.2007.08.030.

Morán-Zenteno, D. J., P. Corona-Chavez, and G. Tolson (1996), Uplift and subduction erosion in southwestern Mexico since the Oligocene: Pluton geobarometry constraints, *Earth Planet. Sci. Lett.*, *141*, 51–65.

Morán-Zenteno, D. J., D. Cerca, and J. Keppie (2007), The Cenozoic tectonic and magmatic evolution of southwestern México: Advances and problems of interpretation, in *Geology of México: Celebrating the Centenary of the Geological Society of México*, edited by S. Alaniz-Álvarez and A. Nieto-Samaniego, *Spec. Pap. Geol. Soc. Am.*, 422, 71–91, doi:10.1130/2007.2422(03).

Morán-Zenteno, D. J., D. J. Keppie, B. Martiny, and E. González-Torres (2009), Reassessment of the Paleogene position of the Chortis block relative to southern Mexico: Hierarchical ranking of data and features, *Rev. Mex. Cienc. Geol.*, *26*, 177–188.

Norman, M., N. Pearson, A. Sharma, and W. Griffin (1996), Quantitative analysis of trace elements in geological materials by laser ablation ICPMS: Instrumental operating conditions and calibration of NIST glasses, *Geostand. Newsl.*, *20*, 247–261.

Onstott, T., and M. Peacock (1987), Argon retentivity of hornblendes; a field experiment in a slowly cooled metamorphic terrane, *Geochim. Cosmochim. Acta*, *51*, 2891–2903.

Oskin, M., and J. Stock (2003), Marine incursion synchronous with plate-boundary localization in the Gulf of California, *Geology*, *31*, 23–26, doi:10.1130/0091-7613(2003)031<0023:MISWPB>2.0.CO;2.

Oskin, M., J. Stock, and A. Martin-Barajas (2001), Rapid localization of Pacific-North america plate motion in the Gulf of California, *Geology*, *29*, 459–462, doi:10.1130/0091-7613(2001)029<0459:RLOPNA>2.0.CO;2.

Passchier, C., and C. Simpson (1986), Porphyroclast systems as kinematic indicators, *J. Struct. Geol.*, *8*, 831–843.

Petrone, C. M., and L. Ferrari (2008), Quaternary adakite—Nb-enriched basalt association in the western Trans-Mexican Volcanic Belt: Is there any slab melt evidence?, *Contrib. Mineral. Petrol.*, *156*, 73–86, doi:10.1007/s00410-007-0274-9.

Pindell, J., and J. F. Dewey (1982), Permo-Triassic reconstruction of western Pangea and the evolution of the Gulf of Mexico/Caribbean region, *Tectonics*, *1*, 179–211, doi:10.1029/TC001i002p00179.

Pindell, J. L., and L. Kennan (2009), Tectonic evolution of the Gulf of Mexico, Caribbean and northern South America in the mantle reference frame: An update, in *The Origin and Evolution of the Caribbean Plate*, edited by K. H. James, M. A. Lorente, and J. L. Pindell, *Geol. Soc. Spec. Publ.*, 328, 1–55, doi:10.1144/SP328.1.

Pindell, J. L., S. C. Cande, W. C. Pitman III, D. B. Rowley, J. F. Dewey, J. Labrecque, and W. Haxby (1988), A plate kinematic framework for models of Caribbean evolution, *Tectonophysics*, *155*, 121–138.

Purdy, E. G., E. Gischler, and A. J. Lomando (2003), The Belize margin revisited. 2. Origin of Holocene antecedent topography, *Int. J. Earth Sci.*, *92*, 552–572.

Ratschbacher, L., et al. (2009), The north American-Caribbean plate boundary in Mexico-Guatemala-Honduras, in *The Origin and Evolution of the Caribbean Plate*, edited by K. H. James, M. A. Lorente, and J. L. Pindell, *Geol. Soc. Spec. Publ.*, 328, 219–293, doi:10.1144/SP328.11.

Roddick, J. (1983), High-precision intercalibration of ^{40}Ar-^{39}Ar standards, *Geochim. Cosmochim. Acta*, *47*, 887–898.

Rogers, R., P. Mann, and P. Emmet (2007), Tectonic terranes of the Chortis block based on integration of regional aeromagnetic and geologic data, in *Geologic and Tectonic Development of the Caribbean Plate in Northern Central America*, edited by P. Mann, *Spec. Pap. Geol. Soc. Am.*, 428, 65–88, doi:10.1130/2007.2428(04).

Ross, M., and C. Scotese (1988), A hierarchichal tectonic model of the Gulf of Mexico and Caribbean region, *Tectonophysics*, *155*, 139–168.

Sandeman, H., D. Archibald, J. Grant, M. Villeneuve, and F. Ford (1999), Characterization of the chemical composition and 40Ar/39Ar systematics of intralaboratory standard MAC-83 biotite, in *Radiogenic Age and Isotopic Studies: Report 12*, *Curr. Res. Geol. Surv. Can.*, *1999-F*, 13–26.

Schaaf, P., D. Morán-Zenteno, M. del S.Hernández-Bernal, G. Solís-Pichardo, G. Tolson, and H. Köhler (1995), Paleogene continental margin truncation in southwestern Mexico: Geochronological evidence, *Tectonics*, *14*, 1339–1350, doi:10.1029/95TC01928.

Scholl, D. W., and R. von Huene (2010), Subduction zone recycling processes and the rock record of crustal suture zones, *Can. J. Earth Sci.*, *47*, 633–654, doi:10.1139/E09-061.

Scholl, D. W., R. von Huene, T. L. Vallier, and D. G. Howell (1980), Sedimentary masses and conepts about tectonic processes at underthrust ocean margins, *Geology*, *8*, 564–568.

Servicio Geológico Mexicano (2007), Carta geológica de la república Mexicana, scale Servicio 1:2,000,000, Pachuca, Mexico.

Silva-Romo, G. (2008a), Guayape-Papalutla fault system: A continuous Cretaceous structure from southern Mexico to the Chortís block? Tectonic implications, *Geology*, *36*, 75–78, doi:10.1130/G24032A.1.

Silva-Romo, G. (2008b), The Guayape-Papalutla fault system: A continuous Cretaceous structure from southern Mexico to the Chortís block? Tectonic implications: Reply (to comment), *Geology*, *36*, e172–e173, doi:10.1130/G25152Y.1.

Solari, L. A., R. Torres de León, G. Hernández Pineda, J. Solé, G. Solís-Pichardo, and T. Hernández-Treviño (2007), Tectonic significance of Cretaceous-Tertiary magmatic and structural evolution of the northern margin of the Xolapa Complex, Tierra Colorada area, southern Mexico, *Geol. Soc. Am. Bull.*, *119*, 1265–1279, doi:10.1130/B26023.1.

Steiger, R., and E. Jager (1977), Subcomission on geochronology: Convention on the use of decay constants in geo- and cosmochronology, *Earth Planet. Sci. Lett.*, *36*, 359–362.

Tao, W., and R. O'Connell (1992), Ablative subduction: A two-sided alternative to the conventional subduction model, *J. Geophys. Res.*, *97*, 8877–8904, doi:10.1029/91JB02422.

Tikoff, B., and D. Greene (1997), Stretching lineations in transpressional shear zones: An example from the Sierra Nevada Batholith, California, *J. Struct. Geol.*, *19*, 29–39.

Tolson, G. (2005), La falla Chacalapa, *Bol. Soc. Geol. Mex.*, *57*, 111–122.

Tolson, G., G. Solis, D.s Moran-Zenteno, A. Victoria, and T. Hernandez (1993), Naturalez petrografica y estructural de las rocas cristalinas en la zona de contacto entre los terrenos Xolapa y Oaxaca, region de Santa Maria Huatulco, Oaxaca, in *Contribuciones a la Tectonica del Occidente de Mexico*, vol. M1, edited by L. Delgado and M. Barajas, pp. 327–349, Union Geofis. Mex., Ensenada.

Tullis, J. (2002), Deformation of granitic rocks: Experimental studies and natural examples, *Rev. Mineral. Geochem.*, *51*, 51–95, doi:10.2138/gsrmg.51.1.51.

von Huene, R., C. R. Ranero, and P. Vannucchi (2004), Generic model of subduction erosion, *Geology*, *32*, 913–916.

Warren, C., C. Beaumont, and R. Jamieson (2008a), Formation and exhumation of ultra-high pressure rocks during continental collision: Role of detachment in the subduction channel, *Geochem. Geophys. Geosyst.*, *9*, Q04019, doi:10.1029/2007GC001839.

Warren, C., C. Beaumont, and R. Jamieson (2008b), Modelling tectonic styles and ultra-high pressure (UHP) rock exhumation during the transition from oceanic subduction to continental collision, *Earth Planet. Sci. Lett.*, *267*, 129–145, doi:10.1016/j.epsl.2007.11.025.

Weyl, R. (1980), *Geology of Central America*, 2nd ed., Gebrüder Bomtraeger, Berlin.
Wilson, J. T. (1965), A new class of faults and their bearing on continental drift, *Nature*, *207*, 343–347, doi:10.1038/207343a0.
Wilson, J. T. (1966), Are the structures of the Caribbean and Scotia arc regions analogous to ice rafting?, *Earth Planet. Sci. Lett.*, *1*, 335–338, doi:10.1016/0012-821X(66)90019-7.

A. J. Hynes, Department of Earth and Planetary Sciences, McGill University, Montreal, Quebec, Canada.

D. F. Keppie, Department of Natural Resources, 3rd Floor, Founders Square, 1701 Hollis St., Halifax, NS B3J 2T9, Canada. (fkeppie@gmail.com)

J. K. W. Lee, Department of Geological Sciences and Geological Engineering, Queen's University, Kingston, ON K7L 3N6, Canada.

M. Norman, Research School of Earth Sciences, Australian National University, Mills Road, Bldg. 61, Canberra, ACT 0200, Australia.